Atmos. Chem. Phys. Discuss.,
https://doi.org/10.5194/acp-2018-409-AC1, 2018

Atmospheric Chemistry and Physics Discussions

Interactive comment on "Daytime HONO, NO_2 and aerosol distributions from MAX-DOAS observations in Melbourne" *by* Robert G. Ryan et al.

Robert G. Ryan et al.

rgryan@student.unimelb.edu.au

Received and published: 9 August 2018

AUTHOR RESPONSES IN BLUE ITALIC TEXT

1. This paper reports measurements of HONO, NO_2 and aerosol using a MAX-DOAS instrument in the city of Melbourne, Australia. It shows enhanced levels of HONO, often peaking in the middle of the day, which would not typically be expected. The authors postulate a ground based photoactivated source of HONO, using evidence based on the dependence of high HONO levels since rainfall, combined with the observed diurnal profiles. It is an interesting paper with potentially significant results in terms of the effect of HONO as an OH source and hence on atmospheric oxidizing capacity. It

Printer-friendly version

Discussion paper

is well written with good, easy to see figures. However, it suffers from the fact that no concurrent other measurements were made, making a full analysis of the effect of HONO on the chemical processes happening difficult. Hence many of the conclusions drawn are based on a bit of speculation which is not ideal. However, the data is of such interest (especially as it contains vertical profiles of HONO) that I do believe it should be published subject to some extra analysis. I realise there is no way to go back and back the extra measurements required but I think there are things that could be done to improve the analysis and conclusions.

We thank the reviewer for their suggestions that lead to improvements of the reactive nitrogen chemistry and exploitation of vertical information provided by the MAX-DOAS, significantly improving the manuscript.

2. One of the great advantages of the MAX-DOAS measurement is that it gives a vertical profile of HONO. Often, measurements are only made at the ground and as HONO is so short lived and postulated sources are often surface based, it is possible that the effect of HONO as an OH source in the entire boundary layer is overestimated. Here, the authors calculate P(OH) from HONO and ozone photolysis and show that in the daytime, OH from HONO is an order of magnitude more than from ozone. However could they do this for the entire vertical profile measurements and hence provide a comparison between the two sources of OH for the entire boundary layer? This would provide an interesting contrast to just looking at the surface data.

In order to compare the OH radical production throughout the troposphere, we have accessed ozone-sonde data collected at the Broadmeadows site which provides temperature, relative humidity and ozone mixing ratio profiles throughout the troposphere (and stratosphere). Using the TUV model, photolysis rates J(HONO) and J(O^1D) were calculated as a function of height through the troposphere. Hence equations 3 and 4 in the manuscript could be used to calculate the OH production rates P(OH) in ppb h^{-1} throughout the troposphere, which are shown in a new figure (now Fig. 9).

It should be noted that in the course of these calculations a mistake was found in the original surface P(OH) calculation and therefore (previously) Fig. 11(e) has been updated. The wrong ozone mixing ratios were used in calculating P(OH, O^1D) meaning that this was underestimated. Accordingly, using the HONO diurnal cycle from 7th March and the appropriate ozone mixing ratios taken from the average EPA values (peaking at 27 ppb) around the city of Melbourne, the OH production due to HONO exceeded that due to ozone by a factor of 4 rather than a factor of 10. The highlighting of the OH production source due to HONO in the abstract of the manuscript has also been changed from reporting a source "up to ten times stronger" to "up to four times stronger".

HONO has previously been observed to be the dominant primary OH production mechanism in urban areas (e.g. Ren et al. (2003); Elshorbany et al. (2009)) using in situ measurements and modelling of surface mixing ratios. Given that the MAX-DOAS technique provides vertical profiles of HONO, the calculation of vertical OH production profiles due to HONO photolysis is possible. With co-located ozone sonde measurements at the Broadmeadows site, primary OH production has been compared across the lowest 8 km of the troposphere in Fig. 9(b). Ozone sonde data has been averaged across all measurements (17 midday measurements, approximately weekly) during the MAX-DOAS measurement period (21 December 2016 to 7th April 2017). This is compared with the average midday HONO profile from the 33 days with peak HONO greater than 0.2 ppb in the lowest retrieval layer. It was assumed that there were no HONO sources above the MAX-DOAS top retrieval height (4 km). HONO Fig. 9(b) shows that while OH production is dominated close to the ground by HONO photolysis, ozone photolysis is dominant above 1 km and will therefore be the dominant OH radical source throughout the whole troposphere. This demonstrates that considering only surface values can give a distorted picture of the relative importance of different radical sources, and highlights the ability of the MAX-DOAS technique to provide important vertically resolved information on tropospheric oxidation chemistry."

3. The authors should also make some comment about other radical sources and how these may compare to the primary OH production from HONO and ozone photolysis (even if they have to estimate what concentration of other species may be).

We have added brief comments on the OH chemistry in response to this comment and point 5 (below). However, in this work we have restricted our study focus to the reactive nitrogen cycle and hence feel that discussion of other radical sources (i.e. VOCs) falls outside the scope of the present paper. Addressing this question with sufficient detail would require emissions data and/or in situ measurements for VOCs, among other species, which are currently lacking for Melbourne. However, given the ability of the MAX-DOAS to measure both ozone and formaldehyde, a key VOC oxidation product, we aim to address this question in future work with an extended MAX-DOAS dataset.

4. I think showing correlation between HONO and NO_2 at different altitudes as well as just at the ground (as in figure 12), would provide some information as to a potential HONO source. Presumably the correlation should get less with increasing height if the HONO source is some form of ground based NO_2 conversion.

This is an interesting idea which was partially explored in the manuscript (previously at Page 13, lines 30-35) when considering the relationship between the retrieved total column and surface values for HONO and NO_2. Here it was found (now using improved regression analysis following comments from Reviewer 2) that the correlation between surface mixing ratio and total column was stronger for HONO than for NO_2 potentially indicating that the HONO source was more likely dominated by the surface than NO_2.

To extend this to the discussion of potential HONO sources as the Reviewer suggests, the correlation between NO_2 and HONO mixing ratios in different retrieval layers was calculated and does indeed decrease with increasing altitude (the table appears in the Supplementary Information Document). However, the interpretation of this finding is not straightforward. While this could indicate conversion of NO_2 at the ground level is contributing to the observed HONO, the same result could equally be interpreted as

being due to the strong vertical HONO gradient due to its shorter lifetime. Furthermore, comparison of correlations at different altitudes from the MAX-DOAS retrieval is complicated by the fact that except for the total column and the lowest retrieval layer, the sensitivity of the retrieval to the measurements (see averaging kernels) is different for NO_2 *and HONO. Furthermore, the work conducted to address point 6 below suggest that* NO_2 *ground conversion cannot bridge the missing daytime HONO source gap, and this point has been added to the discussion.*

In the text of the manuscript, the question has been addressed at (previously) Page 18, lines 19-20, which previously read: "Even if reaction R5 cannot explain the observed HONO levels, the strong correlation of 0.81 between HONO and NO_2 *surface concentrations (fig. 12) suggests that* NO_2 *is implicated in some other way."*

Updated text: "The strong correlation coefficient of 0.81 between HONO and NO_2 *mixing ratios in the lowest retrieval layer (Fig. 10) suggests that* NO_2 *may implicated in the daytime HONO production. The correlation coefficient decreases with increasing altitude (see Table S3 in the Supplementary Information) which could indicate that conversion of* NO_2 *at the ground level is contributing to the observed HONO. However, caution should be taken in interpreting this result since the shorter lifetime and hence expected stronger vertical gradient of HONO compared to* NO_2 *would also lead to a decreasing correlation with altitude. Furthermore, given that the PSS calculation includes the strong* NO_2 *ground conversion rate in Lee et al. (2016) and still cannot replicate the average HONO diurnal profile, photolytic ground* NO_2 *conversion cannot be the dominant daytime HONO producer in Melbourne."*

5. It is a shame there are no NO measurements to allow a steady state and thus a 'missing' HONO concentration to be calculated. However, the authors could make some broad estimate of NO based on their NO_2 measurement and at least a rough estimate of OH concentration and calculate steady state HONO. I think this is important to show how the daytime HONO observed cannot be explained by standard chemistry.

The resulting HONO PSS state concentration is similar in magnitude and diurnal shape to other literature examples , e.g. in London (Lee et al., 2016). A plot of the HONO PSS along with the average observed HONO concentration is now included in the manuscript (part of figure 9), and details of the HONO PSS calculation and result form an updated introduction to Section 3.5 "Possible daytime HONO sources".

6. Some attempt should also be made to calculate the source of HONO from other postulated mechanisms (e.g. surface NO_2 conversion, soil based emission) to give some idea as to whether these mechanisms can produce the daytime HONO observed. Again, it is difficult to do this without some of the supporting data, however estimates could be made based on measurements in other cities in the literature.

Michoud et al., 2014 and Lee et al., 2016 provide useful parameterisations for many different HONO sources including direct HONO emission from traffic, conversion of HNO_3, aerosol-mediated NO_2 to HONO conversion and ground-mediated NO_2 to HONO conversion.

- *Calculating the expected aerosol-mediated conversion of NO_2 requires measurements of aerosol surface area (not available). In addition, as discussed at (previously) page 18, lines 1-6 the observed correlation is low between aerosols and HONO suggesting that aerosol-mediated processes cannot explain the observed HONO.*
- *Neither HNO_3 nor nitrate was measured at Broadmeadows and is very difficult to estimate without appropriate emission factors.*
- *Again, without appropriate emission factors for NO_x, calculating the HONO due to traffic is very difficult however the diurnal cycle of the HONO/NO_2 ratio, which is always > 1%, strongly suggests that traffic emissions cannot explain the observed HONO.*

- *Photoactivated daytime ground conversion of NO_2 is discussed in Lee et al., (2016), and the parameterization therein has been used to estimate the contribution of NO_2 ground conversion in Melbourne. The result now appears in Fig. 9 along with the calculated HONO PSS concentration demonstrating that the PSS + maximal NO_2 ground conversion rate in Lee et al., (2016) cannot explain the observed daytime HONO.*

- *Direct quantification of the soil emission contribution to the observed HONO is impossible without more information on local soil properties ? this is being followed up and will be the subject of further work. However, the contribution can be estimated from (previously) Fig. 13 which shows how the HONO diurnal cycle varies with soil moisture. Since original submission of the manuscript, soil water content percentage (% SWC) has been located through the Australian Bureau of Meteorology which has enabled this figure to be remade using bin values comparable with the literature, rather than the previous arbitrary rainfall index. Comparison along these lines and in response to Reviewer 2 have been added to the Discussion section. In an attempt to show that the missing HONO budget may be closed by soil based emissions, literature values for HONO and NO fluxes have been added to the HONO PSS rate calculation and plotted alongside the observed missing daytime HONO production rate. This now appears in figure 9.*

7. It would be useful to have a table of HONO and NO_2 levels from the literature from other cities round the world. Whilst there is some mention of comparisons in the text it would be clearer if this was brought together in tabular form to allow for easy comparison.

To address this and a similar comment from Reviewer 2, a table of urban HONO and NO_2 measurements reported in the literature has been included in a Supplementary Information document and referenced in the manuscript.

Interactive comment on Atmos. Chem. Phys. Discuss., https://doi.org/10.5194/acp-2018-409, 2018.

Printer-friendly version

Discussion paper

Atmos. Chem. Phys. Discuss.,
https://doi.org/10.5194/acp-2018-409-AC2, 2018

Atmospheric Chemistry and Physics Discussions

Interactive comment on "Daytime HONO, NO_2 and aerosol distributions from MAX-DOAS observations in Melbourne" *by* Robert G. Ryan et al.

Robert G. Ryan et al.

rgryan@student.unimelb.edu.au

Received and published: 9 August 2018

AUTHOR RESPONSES IN BLUE ITALIC TEXT

1. *General remarks: We wish to thank the referee very much for their interest in, and support of, the manuscript as evidenced by their very helpful comments. The suggestions for improved layout, extra references and improved linear regression analyses have greatly improved the flow and quality of analysis in the manuscript.*

2. There is a single major revision to this work that should be made regarding regressions. It is not clear what regression approach the Authors used, but atmospheric

Printer-friendly version

Discussion paper

datasets typically require accounting of error in both measures (e.g. Wu and Yu, 2018). The authors present a Pearson correlation coefficient in Figure 7 and discuss correlations heavily in their discussion from there on. This suggests that a linear least-squares analysis was used, which assumes error in the ordinate alone. The authors should clarify this and present appropriate regression metrics (e.g. slope and regression coefficient) when discussing correlations. Much of the discussion surrounding these comparisons is qualitative while the wording suggest that quantitative evaluations have been made. Including this quantitative information will strengthen the discussion.

The Reviewer is correct in assuming that a linear least-squares method was used in the regression analyses presented, and as such errors in both measures were not appropriately accounted for. To address this, all linear regressions have been recalculated using the Deming regression method, described by e.g. Wu and Yu, 2018, which does allow for errors in both x- and y-variables. The Deming method includes a ratio of variances term (RV) which allows for the comparison of two methods with different inherent random analytical variability. In cases where two variables calculated from the MAX-DOAS retrieval are compared (for example retrieved HONO and NO_2 *surface concentrations) RV has been assumed to be equal to unity. In cases where MAX-DOAS retrieved quantities are compared to external data sources (MAX-DOAS AOD vs MODIS satellite AOD, and MAX-DOAS* NO_2 *concentration vs EPA* NO_2 *in situ data), RV was calculated from the ratio of variances of each technique. Following from the increased confidence in the regression, we have tried to direct the discussion in a more quantitative manner as suggested by the Reviewer. Specific examples are highlighted in further response points below.*

3. Reference to figures throughout the manuscript should be capitalised as 'Fig. X' instead of 'fig. x'. *Corrected. All instances of "fig." have been replaced with "Fig."*

4. Page 3, Lines 30-35: Interferences from clouds, as presented in the discussion, should be included in the drawbacks here.

Corrected. Updated text reads: "However, the MAX-DOAS method has some drawbacks which include complicated, multi-step data processing, limited information content from which to derive vertical profile information and interference from clouds.

5. Page 4, line 30: repetition of 'and' to be corrected

Corrected, thank you

6. Page 5, line 11: differential slant column density is presented here and presumably is the source of the 'dSCD' term used later in the paper. Please define here, if this is correct.

Updated. Text now includes "differential slant column density (dSCD)" for clarity.

7. Page 6, figure 2: Keep the traces in panel c) consistent with the caption. Suggest switching O_3 and HCHO in the caption to be in the same order as the traces.

Caption updated so that HCHO is listed before O_3 as in the figure traces and legend.

8. Figure 2 and Table 1 could be moved to a supporting information document to reduce manuscript length

Figure 2 and Table 1 moved to a Supplementary Information (SI) document as suggested.

9. Figure 3 could be moved to a supporting information document to reduce manuscript length. Figure 4 could be easier to interpret if the time axis is consistent with the others in the manuscript. Two hour time intervals here, and in other diurnal plots, would provide the most detail without becoming cluttered. Figure 4 could benefit from being presented with larger panels if the other figures and table are moved to supporting documentation.

The spectral detection of HONO, as shown in figure 3, underpins the results of the paper and therefore we would like to keep figure 3 in the main body of the text. Figure 4 has been updated to have two-hourly labels on the time-axis, and the panels have

been made larger to aid the reader.

10. Page 8: Section 2.3 is quite long and is detailed for the manuscript, but feels like a lot of detail has also been left out. A suggestion here would be to simplify and condense this section further to improve its clarity (e.g. Equation 1 is not accessible to those not familiar with all of the literature in this section and could be considered superfluous along with many of the details) or some of the details could be moved to supporting documentation and expanded upon in the interests of allowing greater ease of reproduction of this detailed work.

We agree that it is difficult to find the balance in Section 2.3 between accessibility and providing sufficient background mathematical detail to understand the retrieval methods used. In attempting to strike this balance we have re-worded text around equation 1, preferring to leave it in the manuscript as it provides the mathematical context to the discussion of the averaging kernels, degrees of freedom for signal and the retrieval parameter sensitivity tests in section 3.1. The readability of section 2.3 has been improved by shortening it considerably in response to this comment and point 12 below, shifting the latter half to the results section.

*Previous text surrounding equation 1: "In order to retrieve trace gas vertical profiles in this way, information on the atmospheric aerosol extinction is needed to constrain the light path. This is determined using by applying the inversion algorithm to O_4 dSCD measurements. The solution for the aerosol profile **x** is determined iteratively with input aerosol properties being varied so as to minimise the cost function, given by χ^2, i.e. the difference between the measurement vector y and the RTM simulations: ..."*

*Revised text surrounding equation 1: "In order to retrieve trace gas vertical profiles in this way, information on the atmospheric aerosol extinction is needed to constrain the light path. The solution for the aerosol profile **x** is calculated iteratively by varying the aerosol input parameters until the difference between the measurement vector **y** and the RTM simulations is minimised. This difference is given by the cost function χ^2: ..."*

11. Page 8, Line 14: K presented as a weighting function matrix does not appear in either Equation 1 or Equation 2. Please revise.

Corrected. The description of the weighting function matrix K applies to a different form of equation 1, which was included in a previous version of the manuscript. Reference to "K" has now been omitted.

12. Page 9, Lines 9-23: These are results. Suggest relocating to the results and discussion section.

To shorten Section 2.3 and in line with the Reviewer's suggestion, the profile retrieval results shown in (previously) figure 5, and its associated discussion (from page 8 line 10) have been shifted to the Results section. They now form part of Section 3.1 "Vertical distribution of aerosols, NO_2 and HONO".

13. Page 10, Figure 5: There are acronyms (or short-hand notation) being used in the upper row of panels which are not defined in the caption. Please do so. In the bottom row of panels, there are 20 different lines presented in each panel and the values for each are very small in the legend. Are all of these necessary or can half of them be removed without undermining the findings? It would allow all panels in this figure to be increased in size and make it easier to read. Finally, panels (a) and (b) are not labelled here. Please add these.

The averaging kernel labels at the bottom of (previously) figure 5 were indeed busy and have been updated for clarity. Acronyms and short hand notation in the profile figure legends have been replaced with clear and specific labels, the panels have been labelled a, b and c and the caption modified to describe the updated figure.

14. Page 10, Line 4: repetition with 'the"

Repetition removed, thank you

15. Page 10, Lines 13-14: 'by a bias towards the a priori due to lower measurement sensitivity at these levels'. This explanation is unclear. Please consider revising to

improve the clarity here.

Text previously read "The vertical profile reveals a dominant contribution of a priori shape parameters (scale height and ground extinction, blue colours) to upper level uncertainty, with a 60 % error contribution above 500 m. Below 500 m, the influence of the shape parameters is much less significant at 10 %, while the optical properties (yellow and green colours) play a more significant role with a 12 % error. The observed higher sensitivity of the retrieved profiles to the a priori at high altitudes can be explained by a bias towards the a priori due to lower measurement sensitivity at these levels."

This has been revised to: "The vertical profile reveals a dominant contribution of a priori shape parameters (scale height and ground extinction, blue colours) to upper level uncertainty, with a 60 % error contribution above 500 m. This is expected since the inherent higher sensitivity of the retrievals to the measurements at low altitudes, means the a priori profile more strongly constrains the retrieval at high altitudes. Below 500m, the influence of the shape parameters is much less significant at 10 %, while the optical properties (yellow and green colours) play a more significant role with a 12 % error."

As described in point 17 below, this text along with Fig. 6 has now been shifted to the SI document.

16. Page 11, Figure 6: This figure could be moved to a supporting document. The panels are alphabetically labeled, so the text boxes for each can be removed. VCD is not defined in the caption. Also add a note regarding the exponent terms for NO_2 and HONO VCD values as they may be easily missed.

Fig. 6 has been moved to the SI document and labels highlighting vertical column density (VCD) and noting the trace gas column exponent terms have been added to the caption. To further shorten the manuscript, we have decided to move the bulk of Section 3.1 to the SI document since the key finding of the sensitivity tests, namely confidence in the profile retrievals, is summarised by the error shading on the example

profiles in (previously) figure 5. This allows for a more concisely structured results section.

17. Page 11, Line 10: 'the lowest 500m' should be 'in the lowest 500 m'.

Correction made (text now in SI document).

18. Page 11, Lines 11-14: Is the 'high sensitivity' instrumental sensitivity or retrieval sensitivity? Use of the word sensitivity here is a bit unclear and the retrieval sensitivity might be more intuitively termed 'potential error' or 'estimation error' or simply 'error'. What is a 'low error budget'? This wording is not consistent with the rest of this section. Please clarify.

The 'high sensitivity' referred to is the sensitivity of the retrieval to the true profile. 'Low error budget' was perhaps a poorly worded way to indicate that the contribution of errors from a priori and forward model parameters was low. This result is explained in more meaningful detail in what is now Section 3.1. Therefore the revised sentence described below, appearing now in the SI document, has been simplified for greater clarity.

The sentence previously began "The high sensitivity to the ground level retrievals as demonstrated by the HONO and NO_2 *averaging kernels, combined with the low error budget due to smoothing, noise, aerosol and shape a priori parameters in the lowest 500 m, gives confidence in the measured trace gas ground concentrations." This wordy and confusing sentence has been revised to: "The low retrieval errors and high sensitivity to the true atmospheric profile at low altitudes, as demonstrated by the averaging kernels and sensitivity tests presented in (previously) Fig. 5, gives confidence in the measured trace gas surface VMRs".*

19. Page 12, Figure 7: From here on forward, the regression analyses should be clearly presented. A useful quantity that would have been obtained in the analysis here is the slope, which gives some indication of the bias that is discussed qualitatively. Such

bias is expected given that the in-situ monitors are located at ground level (on top of sources), while the MAX-DOAS is observing more dilution of those sources. In the caption of this figure there is a reference to 'surface concentration' measured by the MAX-DOAS, but isn't the lowest elevation angle somewhere between 100 - 500 m above ground level? This isn't terribly clear and could help bridge these observations with ground observations more easily.

We thank the reviewer for the constructive advice regarding the regression analyses. As noted above, the Deming method has now been applied to all regression analyses in the manuscript. This is introduced at (previously) section 3.2 when the MODIS and MAX-DOAS AOD measurements are compared.

Previous text: "Consistent with these limitations, while the ranges for MODIS, averaged over a 10 km spatial radius around Broadmeadows, and MAX-DOAS AOD were very similar (AOD varying between 0.05 and 0.2), the temporal correlation was weak at only 0.33. A longer sampling period and more local compatible datasets, such as PM2.5 measurements, are therefore needed for a useful validation of the MAX-DOAS aerosol 10 results."

Revised text: "Regression analysis was conducted using the Deming method which, unlike simple linear least squares regression, assumes measurement error in both x and y variables. It also allows for the regression to be weighted by the ratio of variances (RV) between the independent and dependent variables. In this case RV ($V_{\mathrm{MAXDOAS}}/V_{\mathrm{MODIS}}$) was 0.37 and the regression analysis showed a slope of 2.18 and Pearson's R coefficient of 0.33. Therefore, while the ranges for MODIS, averaged over a 10 km spatial radius around Broadmeadows, and MAX-DOAS AOD were very similar (AOD varying between 0.05 and 0.2), the MAX-DOAS AOD was typically half the MODIS-retrieved AOD. Addressing such discrepancies between ground and satellite-based retrievals are an important ongoing research area, with longer sampling periods and local compatible datasets such as ceilometer, LIDAR or $PM_{2.5}$ measurements needed for a confident validation of the MAX-DOAS aerosol results."

Further, the reviewer makes a good point regarding the use of the term "surface concentration". In fact, the retrieved quantity is the average mixing ratio over the lowest retrieval layer, which is 0-200 m. This is addressed at (previously) section 3.2 when comparing the EPA and MAX-DOAS NO_2 *VMRs, which now also includes quantitative data from the Deming regression analysis.*

Previous text at page 12, line 16-20: "Given the wide spatial range of the four EPA measurement sites, the possibility for widely varying local meteorological conditions at each site, and the fundamentally different measurement techniques, a correlation of 0.56 is a positive result for this comparison. When the local wind direction at Broadmeadows was from the south-west, correlation between the EPA stations directly to the south-west (Altona North and Footscray) the Broadmeadows MAX-DOAS NO_2 *improved to 0.66, a positive 20 result which provides the strongest external validation available for these the MAX-DOAS trace gas retrievals."*

Revised text: "The Deming regression analysis included an RV $(VAR_{MAXDOAS}/VAR_{EPA})$ *of 1.25 and showed a Pearson's R coefficient of 0.58 and slope of 1.66. The slope of the linear regression highlights that the EPA values are typically higher which might be expected given that the EPA instruments measure in-situ ground level* NO_2 *while the MAX-DOAS "ground VMR" in fact samples the lowest 200 m of the troposphere through which the surface concentration is diluted. Furthermore, given the wide spatial range of the four EPA measurement sites and the possibility for widely varying local sources and meteorological conditions at each site, the correlation of 0.58 is a positive result for this comparison. When the local wind direction at Broadmeadows was from the south-west, correlation between the EPA stations directly to the south-west (Altona North and Footscray) the Broadmeadows MAX-DOAS* NO_2 *improved to 0.66 (although no change in regression slope was observed), a result which provides the strongest external validation available for these the MAX-DOAS trace gas retrievals."*

20. Page 12, Line 9: 2.5 should be a subscript. In addition, wouldn't ceiliometer or

LIDAR measurements be more useful in validating the MAX-DOAS aerosol results?

Subscript added. Indeed, local ceilometer data and LIDAR data would be appropriate, these techniques have been added as suggested - revised text is included in the response to point 19

21. Page 12, Line 17: The technique used by the EPA has not been presented and should be added as supporting instrumentation details in section 2.1. Presumably these are chemiluminescent analyzers with molybdenum converters?

The Reviewer is correct in this assumption, a sentence noting the EPA NO_x measurement technique has been added as suggested.

22. Page 12, Line 19: What is the slope of the comparison? What type of regression was used?

Corrected - addressed in the revision of the regression analyses in Section 3.2, in point 19.

23. Page 13, Lines 6-9: Add appropriate quantitative regression data here, along with coefficient values that justify selection of wording such as 'correlated strongly'. The direction of the correlation is also important. Was the relationship a positive or negative one in each of these cases? Please provide these quantitative details.

The key message here was to show that the colour index had some independent external validation, namely from the solar radiation measurements at Melbourne Airport. Deming regression analysis for the MAX-DOAS colour index vs the mean global irradiance, each parameter being normalised by their respective mean values, gave a slope of 1.75 and Pearson's R coefficient of 0.77, indicating that the values were correlated as expected. Further validation came from the fact that the slope became closer to 1:1 (1.65) and the Pearson's R coefficient increased (0.85) when the cloud filter was applied showing that periods of decreased colour index corresponded with periods of decreased global radiation nearby. Since this is the strongest external validation and

the discussion has been extended, reference to correlation between the HEIPRO retrieval errors and decreased colour index have been removed for clarity and brevity.

24. Page 13, Lines 14-17: These ratios have been derived from measurements made at night or from tunnel studies and their applicability to the interpretation of daytime data is questionable. During the day, the longer lifetime of NO_2 relative to HONO could result in the observed diurnal pattern of HONO/ NO_2 by simple boundary layer mixing processes diluting the surface NO_2 while the surface HONO source does not change (i.e. it could be independent of NO_2, as suggested by the weekend dataset). It may be worthwhile to discuss this further and carry it into the later discussion or to remove HONO/ NO_2 as a suitable daytime metric entirely.

In light of this important point, the discussion around the HONO/NO_2 ratio has been changed. While little can be inferred from the relationship relative humidity and HONO, NO_2 or the HONO/NO_2 ratio (see also discussion of this at point 36 below), there are daytime, ambient air observations to support a HONO/NO_2 ratio < 1 % being indicative of traffic direct HONO emissions (e.g. Elshorbany, 2009). Therefore, at Page 13, lines 14-17 the discussion will focus on the fact that the HONO/ NO_2 ratio allows us to expect a secondary chemical source of the observed HONO, rather than direct HONO emission from the adjacent road corridors. Furthermore, given that Fig. 8 has now been shifted to the SI document, the discussion now centres on the diurnal cycle plots rather than the timeseries plots.

Previous text: "The ratio HONO/NO_2 has been used previously to categorize emission sources of HONO with HONO/NO_2 < 0.01 indicating direct emission dominates HONO production, HONO/NO_2 0.01 to 0.03 indicating NO_2 to HONO conversion at low relative 15 humidity and HONO/NO_2 > 0.03 indicating NO_2 to HONO conversion at high relative humidity (Wojtal et al., 2011; Hendrick et al., 2014; Qin et al., 2009). Figure 8 shows that periods of peak HONO/NO_2 are more commonly a function of low NO_2 than high HONO, and that high HONO corresponds typically to HONO/NO_2 around 0.03."

Revised text (with reference to the diurnal cycle plots now): "The HONO/NO_2 ratio has been used previously to categorize emission sources of HONO with HONO/NO_2 < 0.01 indicating direct emission dominates HONO production (Wojtal et al., 2011; Hendrick et al., 2014; Qin et al., 2009, Elshorbany:2009). Periods of peak HONO/NO_2 were found to be more commonly a function of low NO_2 than high HONO (see also timeseries in Fig. S3 in the Supporting Information), with high HONO typically corresponding to HONO/NO_2 around 0.03. Given that the HONO/NO_2 ratio is consistently greater than 0.01 it is inferred that the observed HONO cannot be attributed to direct traffic emissions from the adjacent road corridors."

25. Page 13, Lines 33-35: Quantitative values for 'correlated strongly'. This is consistent with literature reports of surface processes dominating over aerosol NO_2 conversion. Please cite some examples of this.

Upon checking the mixing layer height (H_{ML}) calculations, it was found that a mistake had been made, using an incorrect conversion factor. With this corrected, the correlation (using the Deming Method) is in fact not very strong, as originally stated, but rather weak with a Pearson's R coefficient of 0.42. The regression analysis shows a slope of 1.65 for HONO vs NO_2 indicating that H_{ML} is typically higher for NO_2 than HONO. This fits with the second original statement that vertical column density and surface mixing ratio correlate more strongly for HONO than NO_2. Similarly, to point 39 below, these findings are both now consistent with previous reports of surface processes dominating HONO production (e.g. Michoud et al., 2014, Lee et al., 2016).

Previous text: "H_{ML} values for NO_2 and HONO correlated very strongly and were consistently shallow at around 500-700 m on sunny days. However, the correlation of vertical column density with surface mixing ratio, which is 0.89 for HONO and 0.80 for NO_2, suggests that surface values are a greater influence on the total column for HONO than NO_2."

Revised text: "Regression analysis using the Deming method showed that H_{ML} values

for HONO and NO_2 were weakly correlated (Pearson's R coefficient 0.42), with a slope of 1.65 indicating that H_{ML} was typically higher for NO_2 than HONO. This is consistent with the correlation of vertical column density with surface mixing ratio, which is 0.89 for HONO and 0.79 for NO_2, suggesting that surface values are a greater influence on the total column for HONO than NO_2. These findings are consistent with previous findings that HONO production is dominated by surface processes rather than at higher altitudes, such as aerosol-mediated conversion of NO_2 (e.g. Michoud et al. (2014); Lee et al. (2016)).

26. Page 14, Figure 8: This figure could be moved to the supporting information document. Remove text boxes on each panel. Label each alphabetically. If necessary, clarify what is on each panel in the caption. Reduce the number of labelled ticks on each ordinate axis.

Figure 8 has been moved to the SI document and changes made to the figure labelling as suggested.

27. Page 14, Figure 9: Change time axis to two-hour intervals. The date format on top of each column is different from that in Figure 8. Keep date formats consistent throughout C5 the manuscript and consistent with ACP guidelines. Remove 'conc.' from the HONO and NO_2 labels. They are correctly identified as mixing ratios in the caption.

Date and time labels have been updated for consistency with other figures, as suggested, and 'conc.' has been removed from the trace gas labels.

28. Page 15, Line 7: Delete 'well'

Corrected, thank you.

29. Page 15, Lines 27-28: These daytime values are higher than might be expected given that the measurement is being made through a large volume and from the NO_2 intercomparison. This would suggest in-situ HONO measurements might exceed 0.5

ppb. How does the > 0.2 ppb HONO value compare to other reports in urban and rural environments?

To address this (and a comment of Reviewer 1) a table of HONO VMRs from urban areas around the world has been compiled and added to the SI document. It can be seen from this table that maximum ground-level HONO VMRs >0.2 ppb can be expected in urban areas. The unusual aspect of the Melbourne measurements is the timing, rather than the magnitude, of the peak. To draw the reader's attention to the table, the text at the start of Section 3.5 has been revised:

Previous text: "During the three month measurement period, 33 days which were mostly sunny had peak HONO concentrations greater than 0.2 ppb. These periods allow analysis of the diurnal cycles of HONO, NO_2 *and aerosol extinction, which are shown in fig. 11."*

Updated text: "During the three month measurement period, 33 days which were mostly sunny had peak HONO concentrations in the lowest retrieval layer greater than 0.2 ppb. From the measurement timeseries (see example timeseries in the Supplementary Information), characteristic ranges for retrieved surface were found to be 0 to 0.35 km-1 for aerosol extinction, 0 to 30 ppb for NO_2 *and 0 to 0.5 ppb for HONO. These values for HONO lie within the range of observed VMRs in urban areas around the world (see Table S2 in the Supplementary Information)."*

The question of these observations compared to rural measurements is addressed at point 33 below.

30. Page 15, Lines 32-33: The authors discuss that HONO does not peak in the early morning during their daylight observations. Are there examples of MAX-DOAS observations capable of seeing the previous night's HONO prior to photolysis? What are the vertical resolution differences between these MAX-DOAS measurements and how might that impact the observations (i.e. if the 'surface' bin is deeper than other observations, you'd expect to observe lower levels). Also, are there limitations in the

MAX-DOAS measurement near sunrise with the instrumental orientation that could result increase the error in capturing a quantitative absorption signal for HONO at this time?

To our knowledge the only previous papers reporting HONO vertical profiles from MAX-DOAS measurements were Hendrick et al., 2014,(Beijing) and Garcia-Nieto et al., 2018 (Madrid). The latter has been published in the intervening period between submission of this manuscript and the Reviewer responses so has now been duly included, with each being cited in several places throughout the manuscript. Hendrick et al present diurnal profiles of HONO VMR from the lowest retrieval layer, for the different seasons. The vertical resolution of the retrieval layers in this paper is the same as in Hendrick et al 2014. In each case the diurnal cycle maximum is at the start of the day, followed by a steady decrease in HONO VMR over the course of the day in line with HONO VMR diurnal cycles in other urban centres measured using different techniques. This suggests that the MAX-DOAS technique can reasonably be expected to detect pre-photolysis morning HONO if it is present.

Nevertheless, retrievals from MAX-DOAS data close to both sunrise and sunset are challenging because sunlight traverses its maximum pathlength through the atmosphere at these times. In the DOAS analysis this is accounted for by optimising fitting parameters (such as choice of DOAS polynomial) and using zenith reference spectra from the most recent set of elevation scans to ensure effective cancellation of stratospheric interference. However it was found that DOAS fit residuals were significantly higher (>1x10-3) for solar zenith angles greater than 80o compared to 4x10-4 for solar zenith angles in the middle of the day, which in turn led to larger differences between modelled and measured dSCDs in the profile retrieval. Hence results are reported for data <80o SZA. Therefore, results presented are missing the first 30 min of daylight in which, potentially, pre-photolysis HONO could exist. Despite this, given that all previous urban HONO diurnal cycles show a decrease across the whole morning, the lack of any morning HONO observed in Melbourne is still considered a significant result.

To clarify this important point the following sentence has been added to (previously) section 3.5: "It should be noted that due to increased DOAS fit residuals and consequent profile retrieval errors for solar zenith angles (SZA) greater than 80o, no data from SZA > 80o is presented. During autumn in Melbourne this means corresponds approximately 30 mins after sunrise and 30 min before sunset."

31. Page 16, Figure 10: Consider moving this figure to a supporting information document. The discussion does a good job of conveying the information presented here.

We believe that Fig. 10 provides an important spatial overview of potential trace gas sources and would like to keep it in the main text.

32. Page 16, Lines 1-5: It would improve the discussion to report the daytime maximum mixing ratios observed in these other locations, for context.

Text previously read: "Previously such daytime maxima in the HONO diurnal cycle have only been observed in rural locations for example at a rural site in Germany (Acker et al., 2006), a forested site in Michigan USA (Zhou et al., 2011), and in rural Cyprus (Meusel et al., 2016) although in each case the peak diurnal HONO value averaged significantly less than observed in Melbourne."

Revised text reads: "Previously such daytime maxima in the HONO diurnal cycle have only been observed in rural locations for example at a rural site in Germany (Acker et al., 2006), a forested site in Michigan USA (Zhou et al., 2011), and in rural Cyprus (Meusel et al., 2016). In each case however, the maximum HONO VMR observed was less than in Melbourne, at 110 ppt, 70 pptv and 100 pptv respectively."

33. Page 17, Figure 11 (and other similar instances): The caption does not describe the panels correctly here. Further, the caption description for the similar panels can be improved by changing the phrase directed for the first panel to the following: 'Diurnal cycle plots for the 1 hourly averages of (a) NO_2, (b) HONO, (c) HONO/NO_2, and (d) aerosol extinction surface values at Broadmeadows'. The alphabetical indicators for

each panel should be displayed outside the axes throughout this figure.

The caption has been updated and the alphabetical labels placed outside the axes as suggested. (Previously) Fig. 12 has also been updated to include (a) and (b) which were missing.

34. Page 18, Line 7: The citations here are not in the proper format to present via 'e.g.'. This is also a hanging sentence. Please correct it.

Corrected. Text previously read: "The HONO diurnal profile observed in this campaign matches temporally with the diurnal profile of the missing HONO production source calculated in both rural e.g. (Meusel et al., 2016) and urban e.g. (Wong et al., 2012; Pusede et al., 2015)."

Revised sentence: "The HONO diurnal profile observed in this campaign matches temporally with the diurnal profile of the missing HONO pro- duction source calculated in both rural (e.g., Meusel et al. (2016)) and urban areas (e.g., Wong et al. (2012); Pusede et al. (2015))."

35. Page 18, Lines 11-18: These ratio values continue to be potentially misleading. Suggest careful revision or even removing this part of the discussion since intensive chemical description of the HONO/NO_2 ratio under sunlit conditions has not been well established.

The reviewer makes a sound point that the discussion of these ratios in sunlit conditions has not been well established. In attempting to understand any relative humidity dependence of the HONO results, the regression analysis presented in this part of the discussion, and the lack of distinct relative humidity trends in the HONO vs NO_2 plot (previously Fig. 12) are stronger evidence. Therefore, discussion of the relative humidity dependent HONO/NO_2 ratios has been removed from this part of the discussion.

Text previously read: "The heterogeneous conversion of NO_2 on wet surfaces accord-

ing to reaction R5 has been suggested as a primary HONO source pathway (Wong et al., 2012) especially during the night when there are no OH radicals available to form HONO via reaction R4. Values of the HONO/ NO_2 ratio between 0.01 and 0.03 have been found when the conversion via reaction R5 proceeds in low relative humidity environments while HONO/ NO_2 > 0.03 indicates 15 conversion at high relative humidity. The average midday HONO/ NO_2 ratio averages around 0.035 (fig. 11(c)) in this case, however fig. 12(b) shows that most of the data points where HONO/ NO_2 is between 0.025 and 0.05 correspond to low relative humidity. The overall correlation between HONO surface concentrations and relative humidity is weak and negative at -0.31 further indicating that reaction R5 cannot explain the high daytime HONO."

Text now reads: "The heterogeneous conversion of NO_2 on wet surfaces according to reaction R5 has been suggested as a primary HONO source pathway (Wong et al., 2012) especially during the night when there are no OH radicals available to form HONO via reaction R4. However, while fig. 12(b) shows that most of the data points for HONO/ NO_2 > 0.025 correspond to relative humidity less than 50 %, there is no clear trend for HONO/NO_2 < 0.025. Regression analysis showed that the overall correlation between relative humidity and HONO VMR was very weak (slope -0.001, coefficient -0.162) further indicating that reaction R5 cannot explain the high daytime HONO."

36. Page 18, Line 20: 'suggests that NO_2 is implicated in some other way'. The weekend data presented here suggests that this may not be true OR that the mechanism is NO_2-saturated. See some discussion of this in (Pusede et al., 2015).

The opening sentence of this paragraph was intended as an introduction to the ensuing discussion of potential NO_2-based HONO sources, rather than a conclusion. To minimise the chance for confusion in relation to this, the paragraph opening "NO_2 is implicated" omitted. The weekend/weekday data is addressed again in this discussion, (previously) page 19 lines 8-13. The good point about NO_2 mechanisms potentially being saturated has been included in the discussion at (previously) lines 8-13 as follows.

Text previously read: "The correlation (between HONO and NO_2) holds as a function of wind speed, with both HONO and NO_2 being localised (fig. 10) although HONO is more dependent on wind direction. As discussed in the source distribution section above, the correlation does not hold between weekends and weekdays and these combined factors suggest that while plausible photo-activated, ground based NO_2 conversion mechanisms exist, the correlation does not necessarily entail high NO_2 to HONO conversion."

Revised text: "While the correlation (between HONO and NO_2) holds as a function of wind speed, HONO is more dependent on wind direction (see Fig. 10) and as discussed above, the correlation does not hold between weekends and weekdays. This suggests that while plausible photo-activated, ground based NO_2 conversion mechanisms exist, such mechanisms may be saturated and or of insufficient strength to account for the observed daytime HONO."

37. Page 19, Figure 13: The data presented here suggest that there is a suppression of HONO daytime surface flux due to increased soil water content. There are a few instances of this hypothesis being tested under laboratory and field conditions that may be worth mentioning here (Donaldson et al., 2013, Donaldson et al., 2014;Oswald et al., 2013;Scharko et al., 2015;Su et al., 2011;Weber et al., 2015). Comparison to the microbial pathways, reversible partitioning, and surface adsorption/dissolution could all enhance the discussion.

Many thanks to the reviewer for these helpful references which show that HONO and NO emissions are indeed expected for dry rather than moist soil. Following this point, along with point 39 and the comments of Reviewer 1, some considerable work has been put in to calculate in greater detail the 'missing HONO budget' in Melbourne. As part of this, modelled soil moisture content data has been obtained from the Australian Bureau of Meteorology which has allowed (previously) Fig. 13 to be remade with bin values comparable to, e.g., Oswald et al., 2013. Furthermore, literature values for potential HONO and NO soil fluxes have been plotted alongside the unknown HONO

production rate to show that soil emissions can plausibly close the local HONO budget. Reference to some the papers suggested above by the Reviewer has been made in this discussion. However given the current length and scope of the manuscript we would like to leave the more focused discussion of possible soil sources, including microbial pathways and partitioning, to a future study containing soil property measurements.

38. Page 19, Lines 1-2: The literature has been clear on the aerosol surface area conversion of NO_2 to HONO being a minor daytime production route for some time. Suggest including some references to the literature that have demonstrated the phenomenon here in support of your findings.

Yes, this has been found before for example in Michoud, et al., 2014 and Lee et al., 2016, citation of these works is now included. Following from the discussion at page 19 lines 1-2, text previously read "indicating that aerosol-mediated NO_2 *conversion cannot explain the observed high daytime HONO levels."*

Revised text: "indicating that aerosol-mediated NO_2 *conversion cannot explain the observed high daytime HONO levels. This is in line with previous findings in, e.g., Michoud et al. (2014) and Lee et al. (2016)."*

39. Page 20, Line 17: This instance of biocrust discussion should be expanded if there are local biocrusts near the observation site, and generally throughout the Melbourne area. The established literature on this, coupled to anything known about regional biocrust microbial composition, may facilitate a stronger capacity to speak on this potential daytime HONO source instead of speculating.

The reviewer is correct in suggesting that the previous discussion around biocrusts was speculative. Indeed, a more detailed description of potential biocrust instances and general soil characteristics in the Melbourne area is being followed up, and will be addressed in future work when more measurements are available. However, the discussion of potential soil-based HONO emissions has been tightened considerably in the re-written section as described at point 37 above and in response to Reviewer

1's extensive suggestions on source term calculations.

Interactive comment on Atmos. Chem. Phys. Discuss., https://doi.org/10.5194/acp-2018-409, 2018.

Daytime HONO, NO_2 and aerosol distributions from MAX-DOAS observations in Melbourne

Robert G. Ryan[1,2], Steve Rhodes[3], Matthew Tully[3], Stephen Wilson[4], Nicholas Jones[4], Udo Frieß[5], and Robyn Schofield[1,2]

[1]School of Earth Sciences, University of Melbourne, Melbourne, Australia
[2]ARC Centre of Excellence for Climate System Science, Sydney, Australia
[3]Bureau of Meteorology, Melbourne, Australia
[4]School of Chemistry, University of Wollongong, Australia
[5]Institute for Environmental Physics, University of Heidelberg, Germany

Correspondence: Robert G. Ryan (rgryan@student.unimelb.edu.au)

Abstract. Nitrogen oxides produced by high temperature combustion are prevalent in urban environments and toxic, contributing to a significant health burden. The chemistry of nitrogen oxides such as NO_2 and HONO in pollution are important for hydroxyl radical production and overall oxidative capacity in urban environments, however current mechanisms cannot explain high daytime levels of HONO observed in many urban and rural locations around the world. Here we present HONO, NO_2 and aerosol extinction vertical distributions retrieved from MAX-DOAS measurements in suburban Melbourne, which are the first MAX-DOAS results from Australia. Using the optimal estimation algorithm HEIPRO we show that vertical profiles for NO_2 and HONO can be calculated with low dependence on the retrieval forward model and a priori parameters, despite a lack of independent co-located aerosol or trace gas measurements. Between December 2016 and April 2017 average peak NO_2 values of 8 ± 2 ppb indicated moderate traffic pollution levels, and high daytime peak values of HONO were frequently detected, averaging 220 ± 30 ppt in the middle of the day. HONO levels measured in Melbourne were typically lower than those recorded in the morning in other places around the world, indicating minimal overnight accumulation, but peaked in the middle of the day to be commensurate with midday concentrations in locations with much higher NO_2 pollution. Regular midday peaks in the diurnal cycle of HONO surface concentrations have only previously been reported in rural locations. The HONO measured represents an OH radical source in the middle of the day in Melbourne up to ~~ten~~ four times stronger than from ozone photolysis. The dependence of the high midday HONO levels on ~~time since rainfall~~soil moisture, combined with the observed diurnal and vertical profiles, provide evidence for a strong photo-activated and ground-based daytime HONO source.

1 Introduction

The World Health Organisation indicates that ambient air pollution exposure presents the largest environmental risk to human health, with as many as one in nine deaths attributable to poor air quality (WHO, 2016). In Australia, with isolated but highly urbanised population centres, the economic burden attributed to health care as a result of air pollution is estimated to be as high as $11 million per year (DEE, 2018). This makes understanding the oxidation chemistry underpinning urban pollution processes, and particularly closing the budget of chemical oxidants in urban areas, a priority for atmospheric scientists. The oxidative capacity of the atmosphere can be defined by its main oxidant, the hydroxyl radical (OH), yet relative contributions of different processes to local and regional OH budgets remains uncertain. Ozone photolysis through R1 and R2 is often considered to be the primary pathway for atmospheric OH formation in the boundary layer:

$$\mathrm{O_3} + h\nu \rightarrow \mathrm{O(^1D)} + \mathrm{O_2} \quad \text{(R1)}$$

$$\mathrm{O(^1D)} + \mathrm{H_2O} \rightarrow 2\mathrm{OH} \quad \text{(R2)}$$

Several studies have identified higher daytime nitrous acid (HONO) levels in urban areas than can be expected from the known mechanisms, indicating an unknown daytime HONO source (Lee et al., 2016; Acker and Möller, 2007; Kleffmann, 2007; Wong et al., 2012; Huang et al., 2017; Neuman et al., 2016). Given that HONO photolysis through R3 is a strong OH production source, elevated daytime HONO levels can increase the local tropospheric oxidative capacity:

$$\mathrm{HONO} + h\nu(300 - 405nm) \rightarrow \mathrm{NO} + \mathrm{OH} \quad \text{(R3)}$$

Major known HONO sources include direct emission from combustion engines, the daytime homogeneous reaction R4, and the heterogeneous reaction R5 occurring on wet surfaces which is believed be the main nighttime HONO source reaction.

$$\mathrm{NO} + \mathrm{OH} + \mathrm{M} \rightarrow \mathrm{HONO} + \mathrm{M} \quad \text{(R4)}$$

$$2\mathrm{NO_2} + \mathrm{H_2O}_{(ads)} \rightarrow \mathrm{HONO} + \mathrm{HNO}_{3(ads)} \quad \text{(R5)}$$

HONO sinks include dry deposition, photolysis to produce OH (R3) and reaction with OH (R6).

$$\mathrm{HONO} + \mathrm{OH} \rightarrow \mathrm{H_2O} + \mathrm{NO_2} \quad \text{(R6)}$$

Since R6 is very slow (rate constant $1.8 \times 10^{-11} s^{-1}$) compared to R3 (photolysis rate J(HONO) $\approx 3 \times 10^{-5} s^{-1}$ around midday) (Sander et al., 2006), photolysis is the dominant daytime sink process. Consequently, HONO accumulating overnight rapidly photolyses in the early morning, and HONO concentrations are expected to decrease with increasing UV radiation. While observing daytime HONO decreases from an early morning maximum, many studies have still observed higher than

expected daytime HONO concentrations, with a missing source component peaking around the middle of the day (Li et al., 2012; Qin et al., 2009; Lee et al., 2016; Hendrick et al., 2014; Pinto et al., 2014). Maximum diurnal HONO mixing ratios have been reported during the daytime in Cyprus (Meusel et al., 2016) and at a rural site in Germany (Acker et al., 2006). Studies have suggested the missing source may be related to heterogeneous chemistry involving water, aerosols, ground surfaces, or soil-based emissions. To assess the feasibility of these potential HONO sources, reliable vertical gradient measurements of HONO and its precursors, including nitrogen dioxide (NO_2) are required. To address this need, in recent times, passive monitoring techniques such as multi-axis differential optical absorption spectroscopy (MAX-DOAS) have risen to prominence.

The MAX-DOAS technique relies on measurements of scattered sunlight in the ultra violet and visible wavelengths (UV-vis), at several different viewing angles, facilitating the retrieval of vertical information on tropospheric aerosol extinction and trace gas concentration (Platt and Stutz, 2008; Hönninger et al., 2004). Variations in light pathlength due to aerosol scattering are inferred from absorption measurements of the oxygen dimer collision complex O_4, which has a well defined relationship with atmospheric pressure (Wagner et al., 2004; Frieß et al., 2006). The retrieved aerosol information can then be used as input to estimate vertical concentration profiles for UV-vis absorbing trace gases including NO_2, HONO, formaldehyde, glyoxal and bromine monoxide e.g. (Vlemmix et al., 2015; Hendrick et al., 2014; Schreier et al., 2016; Jin et al., 2016).

NO_2 has been well studied using MAX-DOAS in many locations around the world due to its strong UV absorbance and its ubiquity as an urban pollutant, e.g. (Ma et al., 2013; Vlemmix et al., 2015; Kanaya et al., 2014; Wagner et al., 2011; Ortega et al., 2015). In contrast nitrous acid has more commonly been studied using active, long-path DOAS due to its lower concentration and weaker absorbance (Platt and Perner, 1983; Kleffmann et al., 2006; Stutz et al., 2010). Recently attention has turned to studying nitrous acid using MAX-DOAS, as shown in a HONO slant column intercomparison during the MADCAT campaign in Mainz, Germany (Wang et al., 2017) and in HONO and NO_2 profile retrievals in Beijing (Hendrick et al., 2014) and Madrid (Garcia-Nieto et al., 2018). The findings of Hendrick et al. (2014) were in line with previous published HONO data from long path DOAS and in situ measurements, showing higher than expected HONO concentrations and indicating an unaccounted source of daytime HONO e.g. (Lee et al., 2016; Acker and Möller, 2007; Kleffmann, 2007; Wong et al., 2012; Huang et al., 2017; Neuman et al., 2016). Considerable efforts have been made to determine the mechanism of the missing source(s), and the importance of HONO as a tropospheric radical source through vertical gradient measurements using long-path DOAS (Stutz et al., 2010; Wong et al., 2012; Young et al., 2012) aeroplanes (Neuman et al., 2016), zeppelins (Li et al., 2014) and towers (Kleffmann et al., 2003; VandenBoer et al., 2013).

Compared to these expensive, short term campaign platforms, MAX-DOAS measurements of HONO vertical profiles as demonstrated in Hendrick et al. (2014) and Garcia-Nieto et al. (2018) have the significant advantages of simple autonomous instrumentation, being cheap to run and able to be deployed in any environment for long term monitoring programs. However, the MAX-DOAS method has some drawbacks which include complicated, multi-step data processing and limited information content from which to draw vertical profile information and interference from clouds. Furthermore, uncertainties in forward model and profile a priori parameters can lead to measurement errors which must be quantified for confidence in the retrieval. While in some locations this is facilitated by co-located aerosol and trace gas measurements, in the absence of such external data, poorly constrained parameters can introduce large errors (Ortega et al., 2016; Wagner et al., 2011).

While MAX-DOAS has been deployed across much of the northern hemisphere, there are few reports of DOAS and HONO observations from the Southern Hemisphere. In this paper measurements are presented from Melbourne which are, to the best of our knowledge, the first MAX-DOAS results published from Australia. Melbourne, the capital of Victoria, is the second largest city in Australia, with over 4.8 million people, accounting for 19% of the national population. The Victorian Environmental Protection Agency (EPA) has been monitoring air quality, including particulate pollution and NO_2 levels at several different sites around the Melbourne metropolitan area since 1979 (see map in ~~fig~~Fig. 1). In that time average annual NO_2 levels have decreased from 13 ppb to below 10 ppb, despite significant population and vehicle number increases (EPA, 2013), attributed to improved vehicle pollution reduction technology and fuel efficiency. With the Australian National Environment Protection Measure Standards annual average NO_2 concentration at 30 ppb, these figures indicate that Melbourne has good air quality as far as nitrogen oxides are concerned. On the one hand, this provides an ideal opportunity to study the oxidation budget of HONO and OH in a low to moderately polluted urban environment. On the other hand, addressing the paucity of air quality data in Melbourne is relevant given that epidemiological studies have demonstrated correlations between particulates and NO_2 pollution on overall mortality (Simpson et al., 2000, 2005) and cardiovascular disease (Barnett et al., 2006) in Melbourne. The results presented in this paper demonstrate the ability of MAX-DOAS measurements to address the air quality data deficit in Melbourne, locally, and the Southern Hemisphere more broadly, and contribute to an improved understanding of how HONO impacts the budget of tropospheric oxidants.

2 Measurement and profile retrieval details

2.1 Measurement site and MAX-DOAS instrumentation

The Australian Bureau of Meteorology (BOM) has operated a MAX-DOAS instrument in Broadmeadows, a northern suburb of Melbourne, since August 2016. Results are presented in this work from December 2016 to April 2017. The instrument is mounted on a laboratory roof looking in a south-westerly direction over one of Melbourne's main arterial motorways (the Western Ring Road) and, further to the south, the northern suburbs and central city as shown in ~~fig~~Fig. 1. Being close to the Western Ring Road, the MAX-DOAS is ideally placed to measure the resulting traffic pollution plumes. Being on the northern fringes of the Melbourne metropolitan area, the instrument is well placed to study the interaction of rural and urban air masses given the appropriate prevailing meteorology.

The MAX-DOAS used in this work was a commercial 1-D instrument manufactured by the German company Environmental Measurement Systems (Envimes). The instrument consists of a scanner telescope box, looking towards a fixed compass direction of 208 degrees, connected by fibre optic and data cables to spectrometer and computer units inside the laboratory. The spectrometer unit contained temperature stablized 75 mm Avantes Spectrometers for UV (295-450 nm, 0.6 nm resolution) and ~~and~~ visible (430-565 nm, 0.6 nm resolution) regions. The UV detector was a Hamamatsu backthinned detector with Schott BG3 fitler and 2048 pixel channels while the visible detector was a Sony 2048L also with 2048 channels. The telescope unit contained a rotating prism and inclinometer facilitating active elevation control with quoted elevation angle accuracy $< 0.1^\circ$. Similar commercial grade Envimes MAX-DOAS instruments have demonstrated good performance at the MAD-CAT inter-

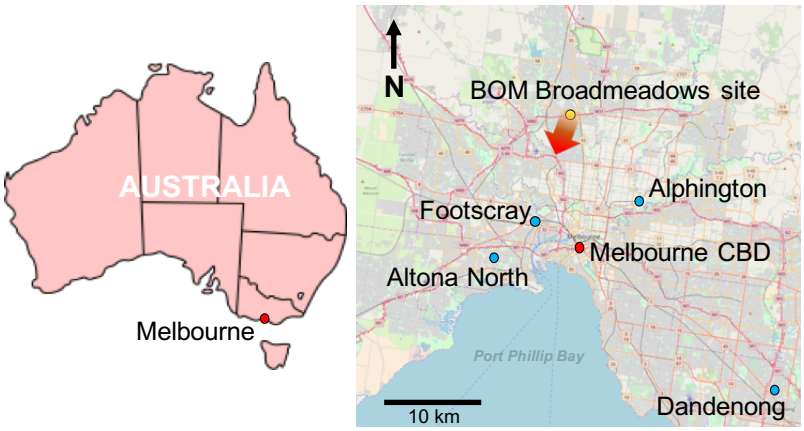

Figure 1. Left: map of Australia showing the location of Melbourne. Right: Map of the Melbourne metropolitan area showing the location of the Broadmeadows measurement site (yellow marker) in the northern suburbs. The red arrow shows the south-south-west viewing direction of the MAX-DOAS instrument. The blue markers indicate the four Victorian EPA NO_2 measurement sites which are referred to in the results section.

comparison campaign in Mainz, Germany (Lampel et al., 2015; Wang et al., 2017). Wavelength calibrations were carried out using an external mercury lamp, and spectra were corrected for detector non-linearity, dark current and spectral offset using laboratory measurements. The measurement sequence was controlled using the MS-DOAS software custom-designed by EnviMes, and consisted of a set of elevation angle scans at 90°, 30°, 20°, 10°, 5°, 3° and 2° which took approximately 12 minutes to complete.

2.2 DOAS fitting

The DOAS technique allows the the Beer-Lambert Law to be applied in an atmospheric context, with 'low frequency' attenuation components of the scattered light spectra (such as Rayleigh and Mie scattering) being separated from the 'high frequency' trace gas absorptions (Platt and Stutz, 2008). The low frequency component is approximated using a polynomial as shown in ~~fig~~Fig. 2(a). The high frequency component is fitted with the relevant trace gas absorption cross sections using a least squares fitting algorithm. The resulting value is the differential slant column density (dSCD), which is the light-path integrated trace gas concentration, relative to a reference spectrum. In the case of MAX-DOAS measurements the reference spectrum is typically the 90° scan recorded as part of a set of measurements at different elevation angles. This reference method cancels out most of the stratospheric influence, allowing the retrieval of tropospheric specific information (Platt and Stutz, 2008).

DOAS analysis was carried out using the QDOAS software developed at BIRA-IASB (http://uv-vis.aeronomie.be/software/QDOAS/). Cross sections used (see table 1) were convolved with the instrumental slit function, measured using mercury emission lines, in QDOAS, and the UV wavelength range 338-370 nm for NO_2 and O_4 were based on recommended settings from the CINDI intercomparison campaign (Roscoe et al., 2010), with the inclusion of the HONO cross section and a temperature dependent

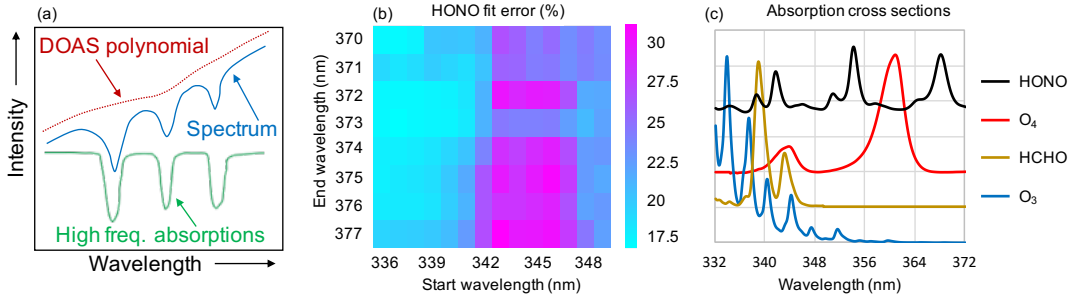

Figure 2. (a) Schematic of the DOAS principle, (b), HONO sensitivity study results using the retrieval interval mapping technique and (c) HONO, O_4, ~~and~~ HCHO and O_3 cross sections plotted between 332 and 372 nm, showing the cross section overlap in the HONO fitting interval.

Table 1. Details of the DOAS settings in this work

Species	Cross section
O_3 (223 and 243 K)	Serdyuchenko et al. (2014)
NO_2 (220 and 298 K)	Vandaele et al. (1998)
O_4 (293 K)	Thalman and Volkamer (2013)
HCHO (297 K)	Meller and Moortgat (2000)
BrO (223 K)	Fleischmann et al. (2004)
HONO	Stutz et al. (2000)
Ring effect (293 K and 250 K)	Grainger and Ring (1962)
DOAS polynomial	5th order
Offset term	1st order

Ring term as in Volkamer et al. (2015); Lampel et al. (2017). A sensitivity study to optimise the HONO fitting wavelength range was performed using the retrieval interval mapping technique of Vogel et al. (2013) (~~fig~~Fig. 2(b)) which showed that the smallest HONO fit percentage errors correspond to a wavelength range starting below 340 nm . When compared to the plot showing all cross sections fitted in the wavelength ranges in ~~fig~~Fig. 2(c), these results show that the HONO fit error is improved by including all three of the largest HONO cross section peaks, including the 341 nm peak which overlaps strongly with formaldehyde (HCHO) and O_4 peaks. This is in line with Wang et al. (2017) and Hendrick et al. (2014), although the fitting window 339-372 nm chosen here for HONO is shorter than in these papers in order to minimise the overall residual RMS of the fits, while maintaining low HONO fit errors.

Successful DOAS retrievals for O_4, NO_2 and HONO are demonstrated in ~~fig~~Fig. 3. In the 339-372 nm fitting window, over the measurement period HONO retrieval errors for solar zenith angles $< 80°$ averaged between 17 % and 25 %, from elevation

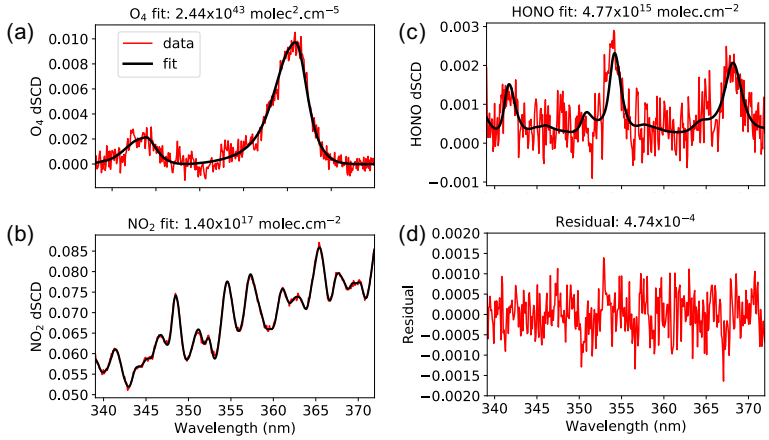

Figure 3. Example DOAS fit results for 2° elevation angle and 28° solar zenith angle on 4th March 2017, showing (a) O_4 and (b) NO_2 in the 338-370 nm fitting window, with (c) HONO and (d) fit residual in the 339-372 nm fitting range.

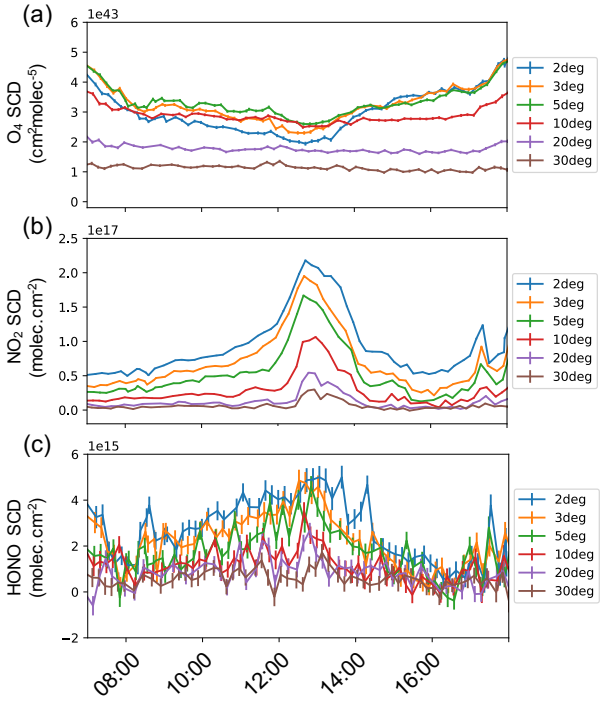

Figure 4. Diurnal differential slant column profiles for (~~top~~a) O_4, (~~middle~~b) NO_2 and ~~HONO~~ (~~bottom~~c) HONO for 4th March 2017.

angles 2° to 30°. These results are not filtered for the influence of clouds. The clear fits shown in ~~fig~~Fig. 3 and separation between dSCDs of different elevation angles shown in ~~fig~~Fig. 4 indicates successful retrieval of HONO slant columns. NO_2 and O_4 fitting errors were typically of order 2 % throughout the measurement period, and residual RMS values averaged $5.37 \times 10^{-4} \pm 1.13 \times 10^{-4}$ but were typically $< 4.8 \times 10^{-4}$ in the middle of the day as in 3(d), for all elevation angles.

2.3 Profile retrieval

A commonly used strategy to retrieve vertical information from MAX-DOAS measurements, involves using a radiative transfer model as a forward model $\mathbf{F}$ to simulate trace gas slant columns. The simulated and measured slant columns are then inverted to calculate a vertical trace gas profile, for example using the optimal estimation method (Rodgers, 1990, 2000; Frieß et al., 2006; Wagner et al., 2004). In order to retrieve trace gas vertical profiles in this way, information on the atmospheric aerosol extinction is needed to constrain the light path. This is determined using by appylying the inversion algorithm to O_4 dSCD measurements. The solution for the aerosol profile $\mathbf{x}$ is determined iteratively with input aerosol properties being varied so as to minimise the cost function, given by χ^2, i.e. the difference between the measurement vector $\mathbf{y}$ and the RTM simulations:

$$\chi^2 = (\mathbf{y} - \mathbf{F}(\mathbf{x}))^T {\mathbf{S}_\epsilon}^{-1} (\mathbf{y} - \mathbf{F}(\mathbf{x})) + (\mathbf{x} - \mathbf{x_a})^T {\mathbf{S_a}}^{-1} (\mathbf{x} - \mathbf{x}_a) \quad (1)$$

In equation 1, $\mathbf{x}_a$ is a priori information which must be provided to constrain the inversion algorithm because the problem is ill-posed. $\mathbf{S_a}$ and $\mathbf{S}_\epsilon$ represent the error covariance matrices of the a priori and measurement vectors respectively~~, while $\mathbf{K}$ is the weighting function matrix which describes the sensitivity of the measurement to perturbations in the aerosol profile~~. The averaging kernel matrix $\mathbf{A} = \frac{\partial \hat{\mathbf{x}}}{\partial \mathbf{x}}$ represents the sensitivity of the retrieved profile $\hat{\mathbf{x}}$ to the true profile $\mathbf{x}$ such that:

$$\hat{\mathbf{x}} = \mathbf{x}_a + \mathbf{A}(\mathbf{x} - \mathbf{x}_a) \quad (2)$$

The information content of a retrieval can be quantified by the degrees of freedom for signal (DOFs), which is the trace of $\mathbf{A}$. The profile retrievals in this work were carried out using the HEIPRO algorithm, as described in Frieß et al. (2006), which uses the radiative transfer code SCIATRAN (Rozanov et al., 2014) as the forward model. HEIPRO also allows for the inclusion of relative intensity measurements in the calculation of aerosol extinction profiles. However, due to the higher sensitivity of intensity measurements to clouds and polarisation, as discussed in Clémer et al. (2010), only O_4 dSCDs were used in the retrieval. To ensure agreement between modelled and measured O_4 dSCDs, simulations in HEIPRO with different cross sectional scaling factors were carried out as in Wang et al. (2016). It was found that a cross sectional scaling factor of 0.80 on the Hermans et al. (2003) O_4 cross section used to model dSCDs in SCIATRAN, consistently brought the measured O_4 dSCDs, fitted using the Thalman and Volkamer (2013) O_4 cross section, into agreement.

Retrieval of NO_2 and HONO profiles in HEIPRO follows the same principles as described for aerosols, where the retrieved aerosol extinction profile for a given scan set of elevation angles is used as input light path information for the trace gas calculations. Aerosol retrievals from O_4 were calculated at 360.8 nm, NO_2 retrievals at 365.4 nm and HONO retrievals at

354.3 nm. HEIPRO was configured to retrieve profiles over 20 layers from 0.1 to 3.9 km, using elevation angle sets of 90°, 30°, 20°, 10°, 5°, 3° and 2°. For all retrievals a fixed exponentially decreasing a priori profile, characterised by a ground concentration (or ground extinction in the case of aerosols) and a scale height was used to initialise the retrieval. A scale height of 0.6 km was chosen for all retrievals, and the surface parameter (i.e. surface extinction for aerosols, surface concentration for trace gases) varied for each retrieved species. The impact of the choice of these a priori and other forward model parameters is discussed in further detail in the results section. Construction of the measurement error covariance matrix $\mathbf{S}_\epsilon$ assumed that measurement errors were independent of each other, with diagonal elements equal to the square of the DOAS fit error. The a priori error covariance matrix $\mathbf{S}_a$ was constructed as described by Frieß et al. (2006) with the variance set to 100 % for all altitudes in order to allow for deviations from the a priori in the case of high aerosol optical depths, while minimising opportunities for the algorithm to fit noise. Figure 5 shows some example retrieval results from HEIPRO, for the 7th of March, a clear sunny day. The profile retrievals are dominated by the layers closest to the ground, as expected given that the averaging kernels show greatest sensitivity in the lowest ≈ 1 km for aerosol extinction and NO_2, and the lowest ≈ 500 m for HONO. The high degrees of freedom for signal (DOFs) found for the aerosol and NO_2 retrieval gives confidence in the retrieval result. While the DOFs for HONO is lower than for NO_2, this result is comparable to the DOFs found for the MAX-DOAS HONO retrieval in Beijing by Hendrick et al. (2014), wherein the difference is attributed to the much greater absorption strength of NO_2 compared to HONO. The combined smoothing and noise errors shown in ~~fig~~Fig. 5 add up to 10% of the retrieved profile in the lowest 500 m for NO_2, and 15% for HONO, in good agreement with the values found in Hendrick et al. (2014). These example vertical profiles are typical for sunny days during the measurement period where aerosol extinction and NO_2 were often found to peak above ground level, and HONO was found to peak at ground level. The location of the measurement site on a hill overlooking the whole city to the south, makes these profile shapes plausible, suggesting that the instrument is typically sampling the particulate and NO_2 pollution plume of Melbourne. The typical HONO profile shape peaking at ground level could be a function of the greater retrieval sensitivity bias for HONO than NO_2 and aerosols. It could also indicate that HONO sources are ground based and highly localised, with strong HONO photolysis not allowing the same daytime vertical gradients as NO_2 and aerosols.

3 Results and discussion

3.1 Aerosol and trace gas retrieval tests

With no appropriate co-located measurements, the choice of a priori and forward model parameters is a source of uncertainty propagating through both the aerosol and trace gas profile retrievals (Ortega et al., 2016; Wagner et al., 2011). In this work, given the lack of independent co-located data sets, a sensitivity study was undertaken to examine the relative contribution of different a priori and forward model parameters on the final aerosol and trace gas retrieval products using the optimal estimation method. The parameters investigated were the surface albedo, aerosol optical properties, aerosol profile shape and trace gas profile shape. The tests involved running aerosol and trace gas retrievals in HEIPRO over three sunny days of measurements at Broadmeadows, varying each parameter separately. Preliminary HEIPRO retrieval runs for March 2017 were used to deter-

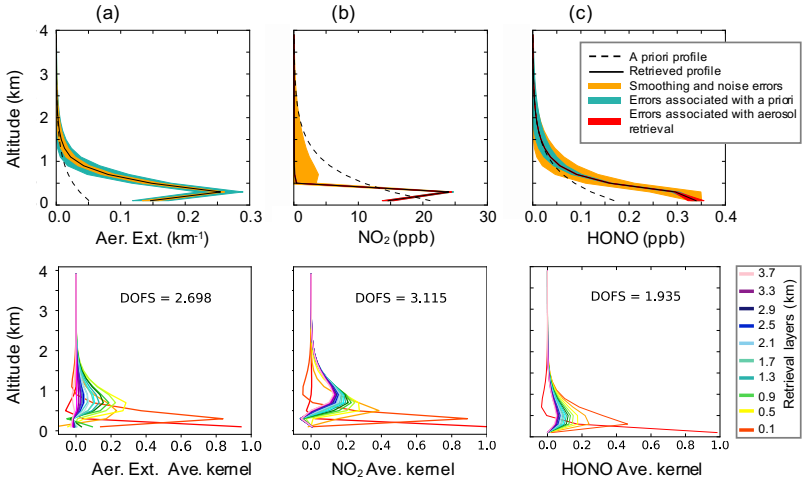

Figure 5. Example profile retrieval results from ~~1300~~ 1 pm (local time) on 7th March 2017 at Broadmeadows, ~~showing~~ for (~~left to right) the~~ a~~priori~~) aerosol extinction, (b) NO_2 and (c) HONO. The top row shows the retrieved profiles, plotted with their associated a priori profile, smoothing and noise errors, and the errors associated with uncertainty in the a priori profile as calculated during the retrieval sensitivity tests. The trace gas profiles also include the error ~~of~~ associated with total uncertainty in aerosol forward model parameters and uncertainty in the aerosol retrieval~~,~~. The bottom row presents the averaging kernels ~~with associated~~ and degrees of freedom for signal ~~and retrieved diurnal aerosol optical depth or vertical column density~~associated with the profile retrieval. ~~(a) shows aerosol extinction results~~The averaging kernels' legend represents the centre wavelength of every second retrieval grid layer, ~~(b) and (c) HONO~~for clarity.

mine ranges for the a priori shape parameters, including scale height ranging from 0.4-0.8 km, and ground extinction ranging from 0.04-0.08 km^{-1}. Ranges for the aerosol optical property tests were determined from AERONET data taken between 2003 and 2017 at six different sites around south eastern Australia, giving Angstrom exponent ranges of 0.3-1.8, asymmetry parameter 0.66-0.75 and single scattering albedo 0.7-1.0, consistent with the ranges discussed for different aerosol types over the Australian continent in Qin and Mitchell (2009). The terrain in the ~~the~~ MAX-DOAS instrument's field of view consists of a grassy field in the immediate vicinity, with roadway, industrial and suburban landscapes beyond, making it difficult to estimate a uniform surface albedo value. For these tests surface albedo range limits of 0.05 and 0.2 were chosen, consistent with field observations of urban surface albedo over grass and motorways respectively (Feister and Grewe, 1995).

Figure 6(a) shows the results from different parameter tests on aerosol optical depth (AOD) and an example aerosol extinction profile from the 7th of March. Each shaded region represents the mean $\pm$ the standard deviation attributable to each test. The vertical profile reveals a dominant contribution of a priori shape parameters (scale height and ground extinction, blue colours) to upper level uncertainty, with a 60% error contribution above 500 m. Below 500m, the influence of the shape parameters is much less significant at 10%, while the optical properties (yellow and green colours) play a more significant role with a 12% error. The observed higher sensitivity of the retrieved profiles to the a priori at high altitudes can be explained by a bias towards the a priori due to lower measurement sensitivity at these levels. The balance of these contributions suggests that a

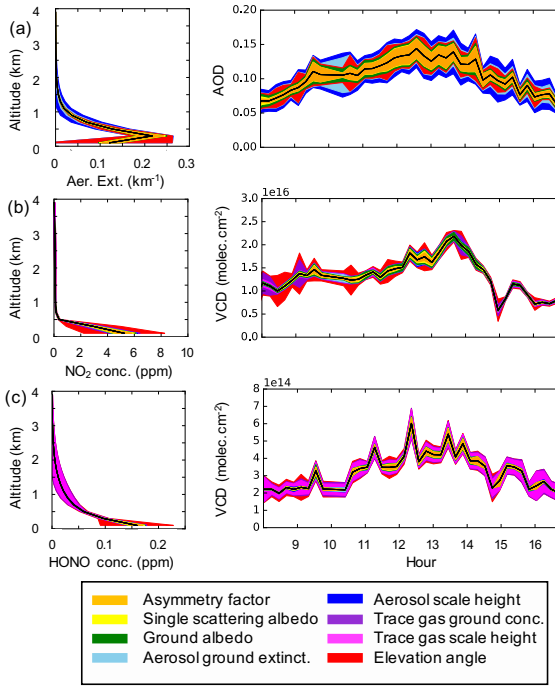

Figure 6. Results of a priori/forward model parameter tests for (a) an example aerosol extinction vertical profile (1 pm local time on 7th March 2017), left, and total aerosol optical depth over the course of the day on 7th March 2017, right; (b) an example vertical concentration profile of NO_2 and NO_2 vertical column density; (c) same as (b) but for HONO. Each colour represents the mean $\pm$ the standard deviation attributable to the particular test parameter as indicated by the legend.

priori shape parameters are a more significant error source than the forward model parameters, as observed in the plot of AOD over the course of 7th March, highlighting that the inherent low sensitivity of MAX-DOAS retrievals to upper levels could be greatly improved with better knowledge of the a priori shape parameters. The combined aerosol errors are included in ~~fig~~Fig. 5 alongside the retrieval smoothing and noise errors. Here it is clear that where the retrieval is most sensitive, in the lowest 500 m, the 17 % error attributable to a priori uncertainty is the most significant error source, compared to the smoothing and noise errors calculated at 6 %. The influence of a $\pm 0.5°$ elevation angle uncertainty, in red, is also included. These results indicate that a $\pm 0.5°$ elevation angle uncertainty leads to a 35 % error in retrieved aerosol extinction close to the ground, and an 11 % error aloft, demonstrating the critical importance of a well calibrated elevation angle to successful MAX-DOAS retrievals.

Figures 6(b) and (c) show the results of the parameter tests on the NO_2 and HONO retrievals. At ground level the elevation angle term dominates the graph, highlighting the importance of elevation angle calibrations for reducing error in retrieved trace gas ground concentrations. The influence of the carry-over aerosol error and trace gas shape a priori parameters is shown to be small, between 3 and 4 % for in each case for both trace gases. This suggests that the HONO and NO_2 ground level concentrations are largely independent of all the aerosol and trace gas parameters, giving confidence in the success of the HEIPRO retrievals. In ~~fig~~Fig. 5 the influence of the aerosol and trace gas a priori and forward model parameters is shown to

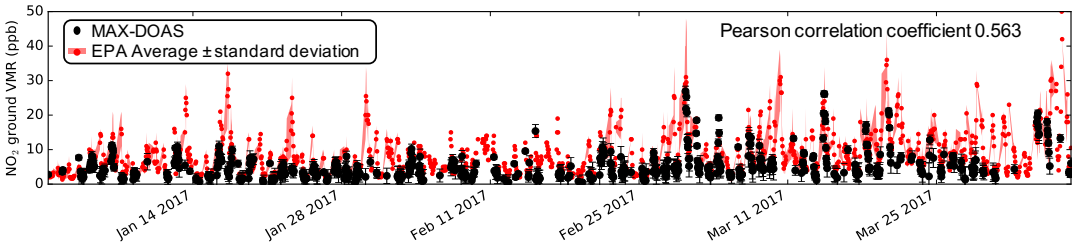

Figure 7. Timeseries comparison of MAX-DOAS measured NO_2 surface concentration at Broadmeadows (black) vs average NO_2 for the four Melbourne EPA monitoring sites (red). All measurements are hourly averages during daylight hours only.

be negligible compared to the retrieval smoothing and noise errors (15 % for HONO and 10 % for NO_2) in the lowest 500m. The high sensitivity to the ground level retrievals as demonstrated by the HONO and NO_2 averaging kernels, combined with the low error budget due to smoothing, noise, aerosol and shape a priori parameters in the lowest 500 m, gives confidence in the measured trace gas ground concentrations. The chemistry and atmospheric pollution implications of these trace gas concentrations are discussed in the following sections.

3.2 Comparison with external data

In the case of Melbourne few options exist for the validation of surface MAX-DOAS data. For aerosol optical depth (AOD) the MAX-DOAS results were compared with AOD retrieval products from the MODIS Terra satellite, at the time of satellite overpass (≈ 1400 local time daily). For a measurement period as short as three months, such comparisons are of limited usefulness since satellite overpasses occur only once a day, and the wavelength of the MODIS 'corrected optical depth' over land was 440 nm while the MAX-DOAS AOD retrieval was at 360 nm in this study. ~~Consistent with these limitations,~~ Regression analysis was conducted using the Deming method which, unlike simple linear least squares regression, assumes measurement error in both x and y variables. It also allows for the regression to be weighted by the ratio of variances (RV) between the independent and dependent variables. In this case RV ($VAR_{MAXDOAS}/VAR_{MODIS}$) was 0.37 and the regression analysis showed a slope of 2.18 and Pearson correlation coefficient of 0.33. Therefore, while the ranges for MODIS, averaged over a 10 km spatial radius around Broadmeadows, and MAX-DOAS AOD were very similar (AOD varying between 0.05 and 0.2), the ~~temporal correlation was weak at only 0.33. A longer sampling period and more~~ MAX-DOAS AOD was typically half the MODIS-retrieved AOD. Addressing such discrepancies between ground and satellite-based retrievals are an important ongoing research area, with longer sampling periods and local compatible datasets ~~, such as PM2.5 measurements, are therefore~~ such as ceilometer, LIDAR or $PM_{2.5}$ measurements needed for a ~~useful~~ confident validation of the MAX-DOAS aerosol results.

While no validation data for HONO was available for Melbourne, the Victorian Environment Protection Agency (EPA) monitors NO_2 mixing ratios at four sites in the Melbourne metropolitan area (Footscray, Alphington, Dandenong and Altona North, as shown in ~~fig~~Fig. 1). The EPA monitors are gas-phase chemiluminescence analysers with molybdenum converters for detection of NO_2, nitric oxide (NO) and total oxides of nitrogen (NO_x). As shown in the timeseries in ~~fig~~Fig. 7 the NO_2

levels measured by the MAX-DOAS at Broadmeadows are generally lower than the average of all four EPA sites over the three month measurement period, however several spikes in the average EPA levels are captured in the MAX-DOAS results such as on January 4th and 6th, and March 1st, 2nd, 4th and 15th. ~~Given the~~ The Deming regression analysis included an RV ($VAR_{MAXDOAS}/VAR_{EPA}$) of 1.25 and showed a Pearson correlation coefficient of 0.58 and slope of 1.66. The slope of the linear regression highlights that the EPA values are typically higher which might be expected given that the EPA instruments measure in-situ ground level NO_2 while the MAX-DOAS "ground VMR" in fact samples the lowest 200 m of the troposphere through which the surface concentration is diluted. Furthermore, given the wide spatial range of the four EPA measurement sites ~~,~~ and the possibility for widely varying local meteorological conditions at each site, ~~and the fundamentally different measurement techniques, a correlation of 0.56~~ the correlation of 0.58 is a positive result for this comparison. When the local wind direction at Broadmeadows was from the south-west, correlation between the EPA stations directly to the south-west (Altona North and Footscray) the Broadmeadows MAX-DOAS NO_2 improved to 0.66 (although no change in regression slope was observed), a positive result which provides the strongest external validation available for these the MAX-DOAS trace gas retrievals.

3.3 Vertical distribution of aerosols, NO_2 and HONO

A three month dataset of MAX-DOAS measurements from Broadmeadows was analysed for aerosol extinction and HONO and NO_2 concentrations. Within this period, results were screened for the likely presence of cloud by applying a filter based on the colour index (CI). The CI was defined as the ratio between spectral intensities at 330 and 390 nm, as in Wagner et al. (2016), for 30° elevation angle scans. The 30° scans were chosen to allow comparison of cloud filtering results with O_4 dSCDs, given that the sequential DOAS referencing method used returns no dSCDs for 90° elevation angles. Diurnal CI thresholds were determined for each of the three months in the campaign period by fitting a 5th order threshold polynomial to CI data from known sunny days as a function of time. Data was filtered out where the CI was less than 10 % of the threshold CI polynomial at the given time, which was found to provide an effective filter for the short analysis period. Despite the lack of colocated external solar radiation data, cloud-flagged periods determined using the MAX-DOAS measured CI filter correlated strongly with periods of low global radiation measured at Melbourne Airport, 6 km west of Broadmeadows. Cloud filtered periods also correlated strongly with high AOD retrieval errors in HEIPRO, giving confidence in the simple empirical cloud filtering approach used here.

A timeseries of retrieved, cloud filtered surface values is shown in ~~fig~~Fig. 8 for aerosol extinction, NO_2 volume mixing ratio (VMR) and HONO VMR. The values shown for this example 13 day period are characteristic of the range of values observed throughout the three months, with ground level aerosol extinction 0 to 0.35 km^{-1}, NO_2 0 to 30 ppb and HONO 0 to 0.5 ppb. ~~The ratio HONO/has been used previously to categorize emission sources of HONO with HONO/< 0.01 indicating direct emission dominates HONO production, HONO/0.01 to 0.03 indicating to HONO conversion at low relative humidity and HONO/> 0.03 indicating to HONO conversion at high relative humidity (Wojtal et al., 2011; Hendrick et al., 2014; Qin et al., 2009). Figure 8 shows that periods of peak HONO/are more commonly a function of low than high HONO, and that high HONO corresponds~~

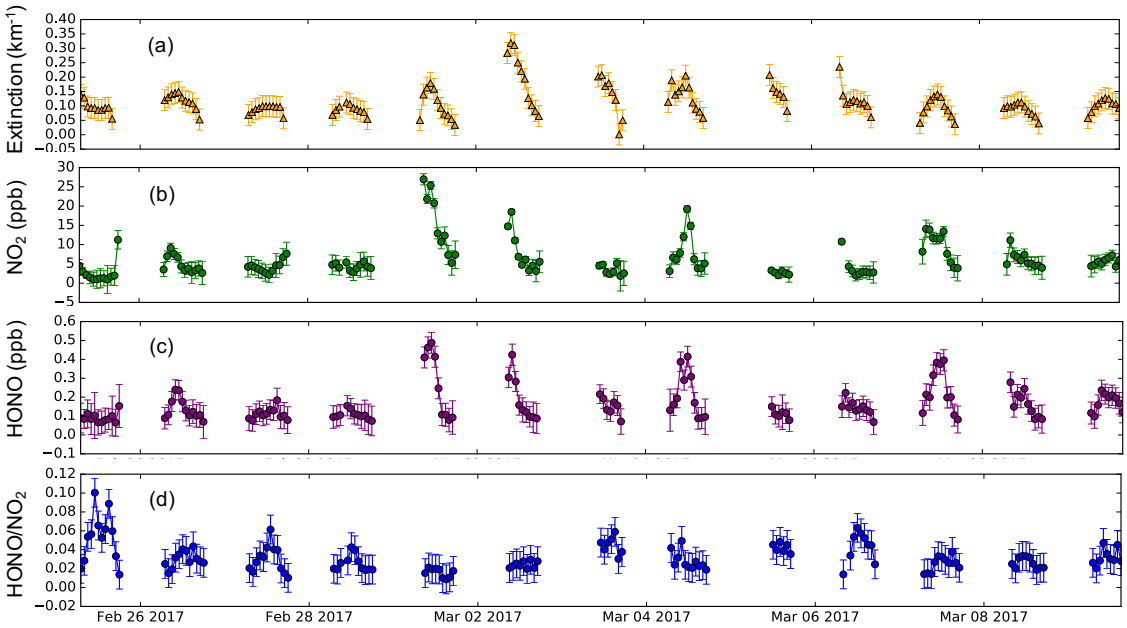

Figure 8. Example timeseries from 25/02/2017 to 10/03/2017 for aerosol optical depth, NO_2 surface concentration, HONO surface concentration and the ratio of HONO/NO_2 surface concentrations

~~typically to HONO/around 0.03.~~ Average diurnal cycles of HONO, NO_2 and HONO/NO_2 will be discussed in more detail in the following section.

The considerable advantage of MAX-DOAS over other methods of measuring HONO is the ability to simultaneously and passively measure vertical distributions of HONO, NO_2 and aerosols. As expected given the profile retrieval sensitivity discussed above, almost all the retrieved aerosol extinction, HONO and NO_2 is in the lower troposphere, as shown in example vertical profile heatmaps in ~~fig~~Fig. 9. The diurnal variation of the aerosol profiles shown on these example days in early March 2017 are typical of the profiles throughout the measurement period. Aerosol extinction commonly peaked temporally in the late morning, and vertically at about 300 m, suggesting that from the elevated measurement position at Broadmeadows the MAX-DOAS is sampling an evolving boundary layer and aerosol pollution plume over the city of Melbourne. NO_2 peaks often correspond well, both temporally and vertically, with aerosol extinction. HONO retrievals are most sensitive to the lowest layer and consequently retrieved HONO peaks are always at the ground level. The strong HONO vertical gradient is also consistent with previous measurements made using various techniques and platforms e.g. ~~(Wong et al., 2012; Hendrick et al., 2014; Stutz et al., 2010; Wong et al., 2012; Young et al., 2012; Neuman et al., 2016; Li et al., 2014; K~~
The presence of periods of peak aerosols and NO_2 above ground level could indicate that they are more likely to be influenced by longer range transport than HONO. Mixing layer heights were estimated as $H_{ML} \approx A \times (VCD/x(ppb))$, following the method of Li et al. (2013), where *x(ppb)* is the trace gas surface mixing ratio and *A* is the conversion factor between molecules.cm^{-3} and ppb. Regression analysis using the Deming method showed that H_{ML} values for HONO and NO_2 were

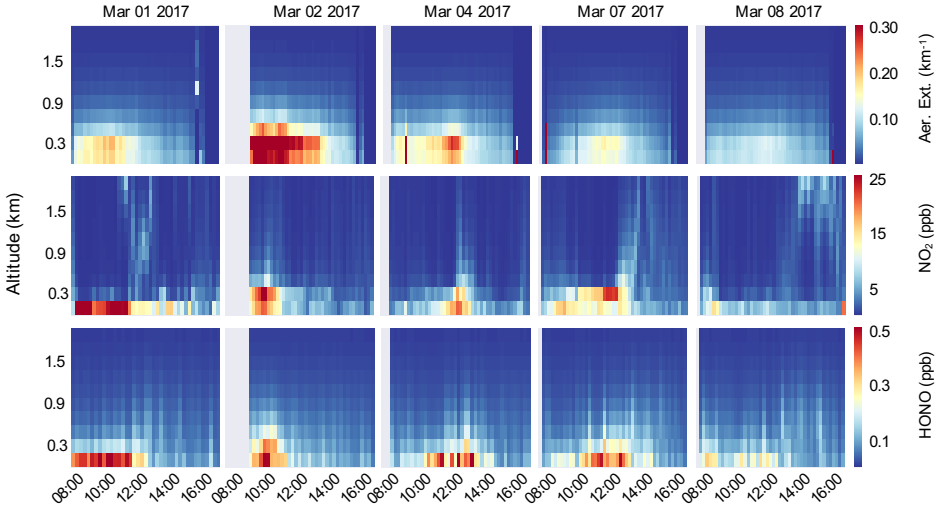

Figure 9. Example vertical profile timeseries, plotted as heatmaps with altitude on the y axis, for selected mostly sunny days in early March 2017. The top row shows aerosol extinction, the middle row NO_2 mixing ratio and the bottom row HONO mixing ratio.

weakly correlated (Pearson's R coefficient 0.42), with a slope of 1.65 indicating that H_{ML} was typically higher for NO_2 ~~and HONO correlated very strongly and were consistently shallow at around 500-700 m on sunny days. However,~~ than HONO. This is consistent with the correlation of vertical column density with surface mixing ratio, which is 0.89 for HONO and ~~0.80~~ 0.79 for NO_2, ~~suggests~~ suggesting that surface values are a greater influence on the total column for HONO than NO_2. These findings are consistent with previous findings that HONO production is dominated by surface processes rather than at higher altitudes, such as aerosol-mediated conversion of NO_2 (e.g. Michoud et al. (2014); Lee et al. (2016)).

3.4 Source distribution of aerosols, NO_2 and HONO

Combining MAX-DOAS measurements of aerosols and trace gases with co-located meteorological observations allows further analysis of spatial source patterns as well as vertical distributions. This is demonstrated using polar bivariate plots where the average trace gas concentrations (~~fig~~Fig. 10(a) and (b)), and aerosol extinction (~~fig~~Fig. 10(c)) is plotted as a function of the wind speed and direction. While this method is not a spatial reconstruction, for this three month data set it allows estimation of the main pollution sources given that low wind speeds corresponds to localised source regions and high wind speeds to pollution transported from further afield. Aerosol extinction, HONO and NO_2 typically show well spatially correlated pollution peaks at low wind speed from the southerly and easterly directions. Using the local map in ~~fig~~Fig. 10 as a guide, we conclude that the major pollution sources are likely to be the Western Ring Road to the south, the busy Camp Road/Sydney Road/Ring Road intersection to the east, and further to the east Victoria's busiest interstate highway the Hume Freeway. These results confirm that pollution is being measured by the MAX-DOAS from the expected sectors. High HONO concentration periods are more

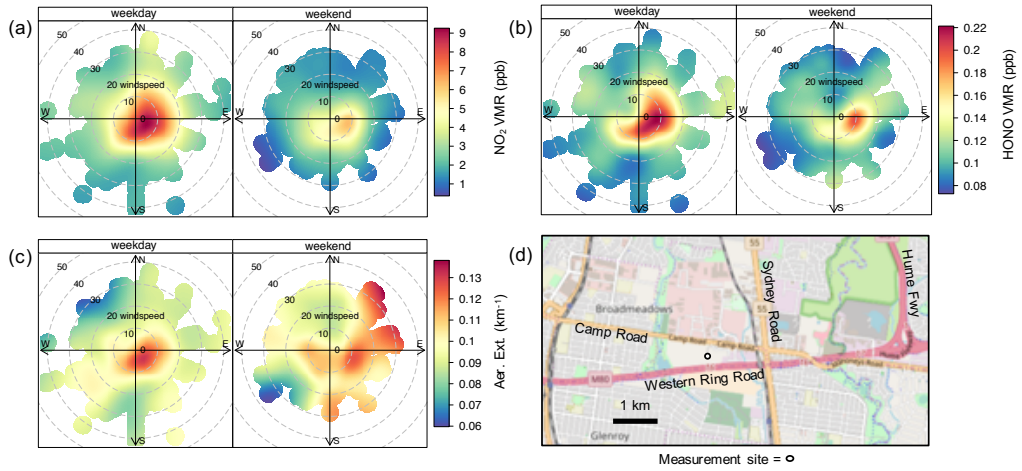

Figure 10. (a) Polar bivariate plot for average weekday (left) and weekend (right) NO_2 surface concentration as a function of wind speed and direction. (b) same as (a) but for HONO, (c) same as (a) but for aerosol extinction and (d) map indicating the location of the major road corridors near the measurement site.

strongly influenced by both wind direction and speed than NO_2 suggesting that the HONO source is more strongly localised to the major road corridors.

The plots in ~~fig~~Fig. 10 are also broken down into weekdays and weekends, showing that weekend NO_2 decreases due to lighter traffic are much more pronounced than for HONO. In fact during March 2017, the most polluted month of the measurement period, the NO_2 average daily concentration halved from 12 ppb during the week to 6 ppb on the weekend, while the HONO average daily concentration falls only from 0.20 ppb to 0.18. A similar phenomenon was found by Pusede et al. (2015) in Pasadena, suggesting that correlations and ratios of NO_2 to HONO needs to be treated with caution when interpreting potential HONO sources.

Surprisingly, localised aerosol sources do not decrease on weekends, and there is an overall increase in aerosol extinction from the north-east sector. This suggests aerosol extinction could be influenced by long range transport, including recycling of pollutants around the Melbourne Metropolitan area e.g. (Pearce et al., 2011), although it is unclear why this would be more apparent on weekends. It is interesting to note that while timeseries and vertical distributions of NO_2 and aerosol extinction are strongly correlated, the differences observed in the spatial distribution provide good evidence that there is no cross correlation in their retrieval.

3.5 Periods of elevated HONO levels

During the three month measurement period, 33 days which were mostly sunny had peak HONO concentrations in the lowest retrieval layer greater than 0.2~~ppb. These periods allow analysis of the~~ ppb. From the measurement timeseries (see example timeseries, Fig. S3 in the Supporting Information), characteristic ranges for concentration in the lowest retrieval layer were

found to be 0 to 0.35 km^{-1} for aerosol extinction, 0 to 30 ppb for NO_2 and 0 to 0.5 ppb for HONO. These values for HONO lie within the range of observed VMRs in urban areas around the world (see Table S2 in the Supporting Information). To further understand the evolution of these species close to the surface over the course of the day, diurnal cycles of HONO, NO_2 and aerosol extinction ~~, which~~ are shown in ~~fig~~Fig. 11. It should be noted that due to increased DOAS fit residuals and consequent profile retrieval errors for solar zenith angles (SZA) greater than 80^o, no data from SZA $> 80^o$is presented. During autumn in Melbourne this corresponds to approximately 30 mins after sunrise and 30 min before sunset. The NO_2 diurnal cycle peaks in the early morning, consistent with morning traffic times on the nearby roadways, remains around 8 ppb throughout the morning before decreasing until the evening traffic period around 5 pm. This diurnal cycle suggests minimal overnight accumulation of nitrogen oxides, a factor which may contribute to the very low observed HONO levels in the early morning (~~fig~~Fig. 11(b)). In other urban studies, HONO during daylight hours typically peaks at sunrise and, despite higher than expected daytime concentrations, decreases across the course of the day. In contrast, the HONO mixing ratio measured here rises from an early morning minimum to a maximum averaging around 220 ppt, one hour before solar noon. Previously such daytime maxima in the HONO diurnal cycle have only been observed in rural locations for example at a rural site in Germany (Acker et al., 2006), a forested site in Michigan USA (Zhou et al., 2011), and in rural Cyprus (Meusel et al., 2016)~~although in each case the peak diurnal HONO value averaged significantly less than observed in Melbourne~~. In each case however, the maximum HONO VMR observed was less than in Melbourne, at 110 ppt, 70 pptv and 100 pptv respectively. Therefore the diurnal maximum HONO measured here is unusual for an urban environment and supports the presence of a strong daytime source.

The ~~average~~ HONO/NO_2 ratio ~~shown in fig. 11(c)exhibits a broad peak between 10 am and midday.~~ has been used previously to categorize emission sources of HONO with HONO/NO_2 < 0.01 indicating direct emission dominates HONO production (Wojtal et al., 2011; Hendrick et al., 2014; Qin et al., 2009, Elshorbany:2009). Periods of peak HONO/NO_2 were found to be more commonly a function of low NO_2 than high HONO (see also timeseries in Fig. S3 in the Supporting Information), with high HONO typically corresponding to HONO/NO_2 around 0.03. Given that the HONO/NO_2 ratio is consistently greater than 0.01 it is inferred that the observed HONO cannot be attributed to direct traffic emissions from the adjacent road corridors. The magnitude of the midday HONO/NO_2 ratio is more consistent with those measured in Cyprus (Meusel et al., 2016) and rural southern China (Li et al., 2012) than urban Beijing (Hendrick et al., 2014), bearing in mind that average peak NO_2 in summer in Beijing is about double that measured here for Melbourne. In fact, while NO_2 levels are low compared to many urban centres around the world, midday HONO concentrations and HONO/NO_2 ratios here are comparable with midday levels reported in Beijing (Hendrick et al., 2014), London (Lee et al., 2016), Pasadena (Pusede et al., 2015) and Houston (Wong et al., 2012) (see also Table S2 in the Supporting Information for a comparison of urban HONO and NO_2 observations from around the world).

The implication of the high daytime HONO levels for the tropospheric oxidation capacity was assessed by comparing the OH radical production rates from HONO photolysis (R3) and ozone photolysis (R1, R2). These are given, respectively, by:

$$P(\mathrm{OH})_{\mathrm{O_3}} = 2 \times f \times J(\mathrm{O}(^1\mathrm{D})) \times [\mathrm{O_3}] \quad (3)$$

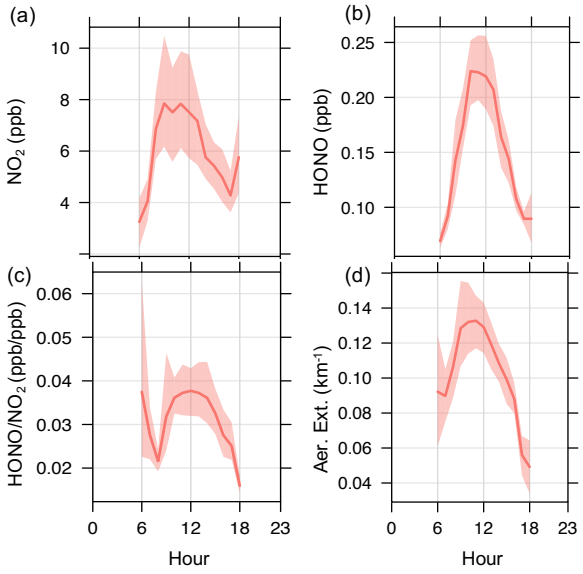

Figure 11. Data from 33 days in the measurement period with high daytime peak HONO. ~~(a)~~ Diurnal cycle ~~plot~~ plots for the 1 hourly averages of ~~HONO surface concentration at Broadmeadows. Solid line shows average value, the shaded region represents the 95 % confidence interval.~~ (~~b) Same as~~ (a) ~~but for the~~ NO_2 ~~surface concentration.~~ , (~~e~~b) ~~Same as~~ HONO, (~~a~~c) ~~but for the surface concentration ratio~~ HONO/NO_2 ~~.~~ , and (d) ~~Same as (a) but for the~~ aerosol ~~ground~~ extinction surface values at Broadmeadows. ~~(c) Diurnal cycle of OH radical production *P(OH)* from ozone (red~~Solid line shows average values, ~~primary y-axis) and HONO (blue, secondary y-axis) photolysis, calculated for an example day with 30 ppb ozone, and the HONO diurnal cycle from 7th March 2018 which peaked near midday at around 400 ppt~~shaded areas are 95 % confidence intervals.

$$P(\mathrm{OH})_{\mathrm{HONO}} = J(\mathrm{HONO}) \times [\mathrm{HONO}] \quad (4)$$

In equation 3, f is the fraction of O^1D reacting with water vapour to form OH (Finlayson-Pitts and Pitts Jr, 1999). $[O_3]$ is the ozone concentration in ppb which was taken from averaged EPA measurements of surface ozone concentration around Melbourne, [HONO] was the ~~surface HONO concentration in ppb calculated~~ VMR in the lowest retrieval layer in ppb, from the MAX-DOAS retrieval. The photolysis rates $J(\mathrm{O}(^1\mathrm{D}))$ and $J(\mathrm{HONO})$ were calculated using the TUV radiation model (Madronich and Flocke, 1999). Photolysis rates were simulated for 7th March 2017, a clear sunny day with a HONO midday peak of 400~~ppt (fig. 8),~~ ppt and Melbourne EPA average O_3 surface concentration 27~~ppb in the late afternoon~~ ppb. The aerosol optical depth was fixed at 0.15 (from the MAX-DOAS aerosol retrieval), and the total ozone column was fixed at 270 D.U. consistent with zenith DOAS measurements using the same MAX-DOAS instrument. The TUV simulated $J(\mathrm{O}(^1\mathrm{D}))$ values were consistent with the empirical parameterisation of Wilson (2015) for $J(\mathrm{O}(^1\mathrm{D}))$ at Cape Grim in north-western Tasmania. The resulting $P(\mathrm{OH})$ diurnal values are presented in ~~fig. 11(e~~Fig. 12(a), showing that the peak OH production rate in the middle of the day ~~is around 0.2~~ was estimated at 0.5 ppb h^{-1} from O_3 photolysis, and on the 7th of March was around 2 ppb

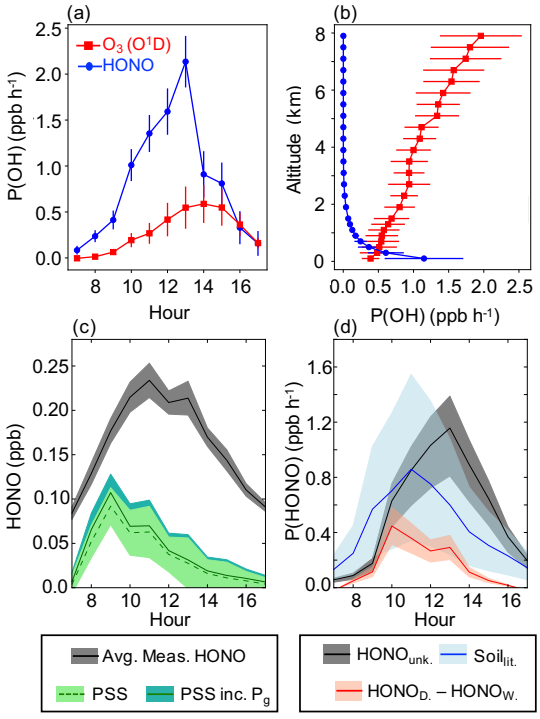

Figure 12. (a) Diurnal cycle of ground level OH radical production *P(OH)* from ozone (O_3 to $O(^1D)$) and HONO photolysis, calculated for an example day with 27 ppb surface ozone, and the HONO diurnal cycle from 7th March 2018 which peaked near midday at around 400 ppt. (b) Vertical profiles of tropospheric OH radical production from HONO photolysis, calculated using the average measured HONO vertical profile and from ozone photolysis calculated using colocated ozone sonde data averaged from January to April 2018. Points represent the mean, errorbars represent one standard deviation. (c) Measured average HONO diurnal cycle plotted with calculated photostationary state (PSS) HONO concentration and PSS including NO_2 ground conversion term (PSS inc. P_g). (d) $HONO_{unk.}$: unknown HONO production rate (measured - PSS), $HONO_D - HONO_W$: measured HONO emission rate attributable to soil processes (driest conditions - wettest conditions, see Fig. 14 and discussion in Section 3.5) and $Soil_{lit.}$ representing PSS + literature HONO and NO soil emission rates. Lines represent means, shaded regions represent 95 % confidence intervals.

h^{-1} from HONO photolysis. Note that since the HONO mixing ratios are calculated throughout the lowest retrieval layer (0-200 m) the ground surface mixing ratios, and therefore the OH production rates, are likely to be larger. This suggests that that HONO levels at 400 ppt in the middle of the day can increase the local OH radical production by ~~an order of magnitude~~up to a factor of four, significantly increasing the local tropospheric oxidative capacity in Melbourne. For the 33 days with high daytime HONO peaks, the average diurnal cycle peak of [HONO] at 220 ppt corresponds to a source of OH radicals around 1 ppb h^{-1}, ~~five times greater than~~ double that from ozone photolysis.

HONO has previously been observed to be the dominant primary OH production mechanism in urban areas (e.g. Ren et al. (2003); Elshor using in situ measurements and modelling of surface mixing ratios. Given that the MAX-DOAS technique provides vertical

profiles of HONO, the calculation of vertical OH production profiles due to HONO photolysis is possible. With co-located ozone sonde measurements at the Broadmeadows site, primary OH production has been compared across the lowest 8 km of the troposphere in Fig. 12(b). Ozone sonde data has been averaged across all measurements (17 midday measurements, approximately weekly) during the MAX-DOAS measurement period (21 December 2016 to 7th April 2017), and included temperature, pressure and relative humidity which enabled water mixing ratios to be estimated throughout the troposphere. The resulting vertical O_3 to O^1D OH production profile is compared with that expected from the average midday HONO profile throughout the campaign, assuming that no extra HONO sources existed above the MAX-DOAS top retrieval height (4 km). HONO Fig. 12(b) shows that while OH production is dominated close to the ground by HONO photolysis, ozone photolysis is dominant above 1 km and will therefore be the dominant OH radical source throughout the whole troposphere. This demonstrates that considering only surface values can give a distorted picture of the relative importance of different radical sources, and highlights the ability of the MAX-DOAS technique to provide important vertically resolved information on tropospheric oxidation chemistry.

3.6 Possible daytime HONO sources

The HONO diurnal profile observed in this campaign matches temporally with the diurnal profile of the missing HONO production source calculated in both rural (e.g. ~~(Meusel et al., 2016) and urban~~ , Meusel et al. (2016)) and urban areas (e.g. ~~(Wong et al., 2012; Puse~~ , Wong et al. (2012); Pusede et al. (2015)). In order to determine the magnitude of the unknown HONO concentration in Melbourne, a simple photostationary state (PSS) calculation has been performed following the example of Kleffmann (2007).

$$[\mathrm{HONO}]_{PSS} = \frac{k_1[\mathrm{OH}][\mathrm{NO}] + P_g}{k_2[\mathrm{OH}] + J(\mathrm{HONO})} \quad (5)$$

The temperature dependent rate constants k_1 and k_2 are for reactions R4 and R6 respectively, and have been calculated according to the parameterisations in Atkinson et al. (2004). Unfortunately, no hydroxyl radical (OH) or nitric oxide (NO) measurements were available at the measurement location during the campaign ~~precluding the calculation of expected photo-stationary state HONO concentrations and the magnitude of relative source contributions. Nevertheless comparing the~~ . To enable a PSS estimate, OH concentrations have been estimated using a simple box model which has been initialised using pollutant emissions data from Sydney in the absence of up-to-date emissions data for Melbourne. Simulated OH radical concentrations peaked at 0.07 ppt in the middle of the day in good agreement with measured background OH levels at Cape Grim in north-western Tasmania, to the south of Melbourne (Creasey et al., 2003). NO concentrations are measured by the Victorian EPA in conjunction with NO_2 at four monitoring sites around metropolitan Melbourne, and from these NO and NO_2 measurements an average diurnally varying NO/NO_2 ratio was calculated. The local NO concentration at the MAX-DOAS ~~measurements with co-located meteorological data provides insight into possible source mechanisms for the high daytime HONO concentrations~~measurement site was then estimated as $NO_{local} = NO_{2local} \times (NO/NO_2)_{EPA}$. As in Michoud et al. (2014), the PSS equation can be expanded from considering only the photo-chemistry by including additional parameterised HONO source or sink terms in the PSS numerator or denominator respectively. In equation 5, P_g represents an additional source term due to ground conversion

of NO_2 where $P_g = k_c \times 0.25 \times J(NO_2) \times [NO_2]$ and $0.25 \times J(NO_2)$ is the scaled NO_2 photolysis rate calculated using the TUV model (Lee et al., 2016). The ground conversion rate k_c has been set to 6×10^{-6}, which was found in Lee et al. (2016) to be the average ground conversion rate necessary to close the missing HONO budget in London. As seen in Fig. 12(c), the calculated HONO PSS concentration underestimates HONO levels especially in the middle of the day and the afternoon, consistent with previous observations in both rural (e.g. Meusel et al. (2016)) and urban (e.g. Michoud et al. (2014); Lee et al. (2016)) environments.

HONO and NO_2 mixing ratios are strongly correlated (Pearson's R=0.81) in the lowest retrieval layer as shown in Fig. 13. The Pearson's R coefficient decreases with increasing altitude (see Table S3 in the Supporting Information) which could indicate that conversion of NO_2 at the ground level is contributing to the observed HONO. However, caution should be taken in interpreting this result since the shorter lifetime and hence expected stronger vertical gradient of HONO compared to NO_2 would also lead to a decreasing correlation with altitude. Furthermore, given that the PSS calculation includes the strong NO_2 ground conversion rate in Lee et al. (2016) and still cannot replicate the average HONO diurnal profile, photolytic ground NO_2 conversion cannot be the dominant daytime HONO source in Melbourne. The heterogeneous conversion of NO_2 on wet surfaces according to reaction R5 has been suggested as a primary HONO source pathway (Wong et al., 2012) especially during the night when there are no OH radicals available to form HONO via reaction R4. ~~Values of the HONO/ratio between 0.01 and 0.03 have been found when the conversion via reaction R5 proceeds in low relative humidity environments while HONO/> 0.03 indicates conversion at high relative humidity. The average midday HONO/ratio averages around 0.035 (fig. 11(c)) in this case, however fig.~~ However, while Fig. 13(b) shows that most of the data points ~~where~~ for $HONO/NO_2$ ~~is between~~ > 0.025 ~~and 0.05 correspond to low relative humidity . The~~ correspond to relative humidity less than 50 %, there is no clear trend for $HONO/NO_2$ < 0.025. Regression analysis showed that the overall correlation between ~~HONO surface concentrations and relative humidity is weak and negative at -0.31~~ relative humidity and HONO VMR was very weak (slope -0.001, Pearson's R coefficient -0.16) further indicating that reaction ~~R5~~ R5 cannot explain the high daytime HONO.

~~Even if reaction R5 cannot explain the observed HONO levels, the strong correlation of 0.81 between HONO and surface concentrations (fig. 13) suggests that is implicated in some other way. One mechanism could involve photo-enhanced~~ Photo-enhanced uptake and conversion of NO_2 on aerosols, such as organics, ~~as proposed by George et al. (2005)~~has been proposed as a daytime HONO source (e.g. George et al. (2005)). Only moderate temporal correlations of 0.58 and 0.49 between aerosols and HONO were found for surface and total column amounts respectively. In addition, HONO and aerosol vertical distributions were often different as indicated in figures 5 and 9, indicating that aerosol-mediated NO_2 conversion cannot explain the observed high daytime HONO levels. This is line with previous findings in, e.g., Michoud et al. (2014) and Lee et al. (2016). This argument also suggests that photodissociation of particulate nitrate, which was found to be a HONO source with a diurnal peak before midday by Ye et al. (2017), is not the major daytime HONO source here.

While the diurnal cycles of HONO and $HONO/NO_2$ indicate a more 'rural' type of HONO production, the high HONO to NO_2 correlation in Melbourne matches what is expected in an urban setting (Hendrick et al., 2014). ~~The~~ While the correlation holds as a function of wind speed, ~~with both HONO and being localised (fig. 10) although HONO~~ HONO is more dependent on wind direction ~~. As discussed in the source distribution section~~ and as discussed above, the correlation does not hold between

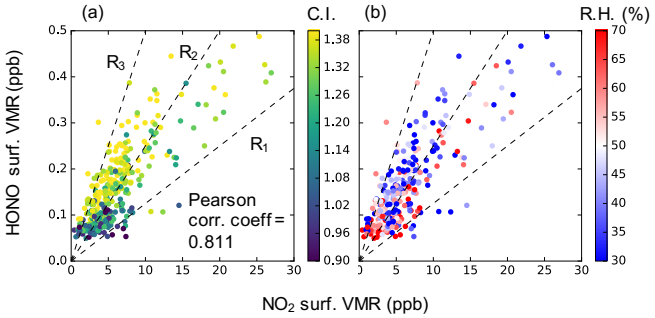

Figure 13. Scatter plots of (a) HONO ground concentration vs NO_2 ground concentration coloured by colour index (CI), showing dependence of high HONO values on solar radiation. Note that CI is the ratio of intensities measured by the MAX-DOAS instrument at 330 and 390 nm. The cloud filtered CI correlated strongly with global irradiance measured 6 km to the west at Melbourne Airport. (b) HONO ground concentration vs NO_2 ground concentration coloured by relative humidity. Dashed lines represent the ratios R_1 HONO/NO_2 = 0.0125, R_2 HONO/NO_2 = 0.025 and R_3 HONO/NO_2 = 0.05.

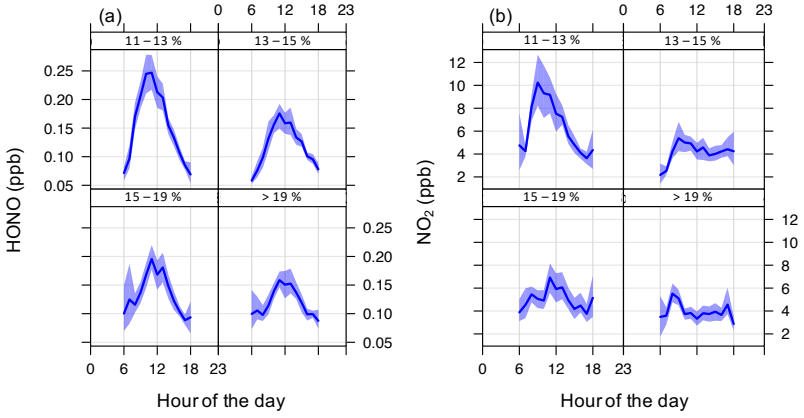

Figure 14. (~~Left~~a) HONO and (~~right~~b) NO_2 diurnal cycles over the three month measurement period, divided into four ~~rainfall index bins where lowest rainfall index indicates days likely to have lowest~~ soil ~~moisture, and highest rainfall index indicates days with highest soil moisture~~water content (SWC) % bins. SWC data has been obtained from the Australian Water Resources Assessment Modelling System.

weekends and weekdays~~and these combined factors suggest~~. This suggests that while plausible photo-activated, ground based NO_2 conversion mechanisms exist, ~~the correlation does not necessarily entail high to HONO conversion~~such mechanisms are either saturated and/or of insufficient strength to account for the observed daytime HONO.

Therefore other mechanisms, ~~disconnected from~~ independent of NO_2, may be contributing to the daytime HONO formation. Processes at the ground surface have been suggested to provide strong daytime HONO sources, including nighttime deposition of HONO or gaseous atmospheric acids to a surface reservoir followed by daytime re-emission (VandenBoer et al., 2014, 2015), and photoactivated reactions involving humic acids (Stemmler et al., 2006) and soil nitrites (Su et al., 2011).

Such ~~a~~ ground-based sources match both the strong vertical HONO gradients and diurnal profile of the daytime HONO observed in Melbourne, suggesting that these mechanisms could explain the presence of HONO in the middle of the day. Lee et al. (2016) concluded that in London, the highly urbanised environment surrounding the measurement site meant soil-based HONO contributions were unlikely to contribute to the observed high daytime HONO budget. In contrast, the ~~outer-suburban~~ Broadmeadows measurement site is surrounded by a variety of surfaces including vacant fields, wide grassed road verges, medium density outer-suburban development and parkland and consequently soil-based processes must be considered in the possible daytime HONO formation mechanisms.

Meusel et al. (2018) showed that in Cyprus~~HONO~~ , emissions from soil ~~biocrusts could explain the daytime~~ and soil biocrusts could maximally explain 85 % of the local daytime missing HONO source. Measurements of reactive nitrogen fluxes from bacteria in soil biocrusts by Weber et al. (2015) and Meusel et al. (2018) found that optimum HONO ~~budget. They also found that NO was emitted from soil biocrusts~~ and ~~that maximum HONO and~~ NO emission ~~was observed for bare soil with moisture contents around 25 % . With no soil measurements available during this campaign, a simple approximation for soil moisture content was made by considering how HONO and~~ conditions were between 20-40 % soil water content (SWC), while Oswald et al. (2013) showed that maximum reactive nitrogen flux from a range of soil samples around the world occurred at around 10 % SWC. In order to test the potential role of soil emissions on the HONO budget in Melbourne, modelled soil moisture data has been obtained from the Australian Water Resources Assessment Modelling System (Hafeez et al., 2015). Figure 14 shows a clear variation in midday HONO and NO_2 ~~diurnal cycles changed in relation to the timing and amount of rainfall. An empirical rainfall index was defined for each day according to $RI = 100 - D_{pr}/R_{pd}$, where the rainfall index on a day with any rain is arbitrarily defined as $RI = 100$, D_{pr} is the number of days since the previous rainfall event (i.e. $D_{pr} = 0$ if raining today, $D_{pr} = 1$ if it rained yesterday, and so on) and R_{pd} is the amount of rainfall, in mm, in the most recent rainfall event. Rainfall on consecutive days was defined as one rainfall event, with R_{pd} being the sum of all rainfall in that event. RI, and hence assumed soil moisture , was therefore a maximum, 100, on rainy days decreasing to a minimum when (a) it had not rained for many days and or (b) the previous rainfall amount was small. Figure **??** shows that the average HONO diurnal cycle daytime maximum was much higher when the soil was likely to be dry, rather than wet, suggesting that daytime HONO in Melbourne may indeed depend on soil moisture. These findings are consistent with the low HONO emissions from biocrusts at very high soilmoisture content as discussed in Meusel et al. (2018). In that paper, very low soil moisture were predicted to result in decreased HONO production efficiency. Such a decrease inpeak HONO values is not observed here, possibly due to the frequency of rainfall events during the campaign or the nature of the local soil biocrusts. Interestingly the same trend was observed for~~ levels with soil moisture, suggesting that reactive nitrogen emissions from the soil may be a key factor in both HONO and NO levels. With decreases in midday HONO (and potentially NO, given the NO_2 ~~which suggests that periods with peaking in the~~ trend) above 11 % SWC these results correspond with dependence of reactive nitrogen emissions from soil, as in Oswald et al. (2013) than from biocrusts as in Meusel et al. (2018) and Weber et al. (2015).

The soil mediated HONO production rate in ppb.h^{-1} could be estimated by looking at the difference between the production rates in the driest and wettest SWC bins, as shown in red in Fig. 12(d). This rate closes the HONO budget in the morning but not in the middle of the day ~~may be attributable to~~ or afternoon. To test whether soil based processes could close the whole budget,

an updated $HONO_{PSS}$ has been calculated by including the diurnal cycle of soil HONO and NO soil emissions from Cyprus, presented in Meusel et al. (2018). Shown in blue in Fig. 12(d), large shaded error margins on this plot indicate the wide range of observed HONO and NO fluxes from the Cyprus samples. Comparison with Melbourne is complicated by the dependence of HONO and NO fluxes on a wide variety of other soil parameters outside the scope of this study, including soil properties, pH and temperature. Nevertheless the comparison suggests that soil emissions have the potential to bridge the midday and afternoon gap in HONO production rate, providing strong evidence that it would be worthwhile investigating soil-based ~~NO production rather than traffic emissions. This is highlighted by the diurnal cycles in the two wettest *RI* bins which show early morning increases consistent with morning peak traffic times, but do not go on to match the high midday levels seen in the two driest *RI* bins. These preliminary findings point to an important role for soil-based emissions in the observed level of nitrogen oxides, however NO , soil moisture, chemistry and biology measurements, as well as a longer measurement period, will be necessary to determine the responsible soil based mechanisms in~~ reactive nitrogen emissions in Melbourne.

4 Conclusions

~~This study reports~~ Here we report on the first MAX-DOAS measurements from Melbourne, Australia ~~.~~ (37.7° S, 144.9° E), from December 2016 to November 2017. A detailed uncertainty analysis of the retrieval a priori and aerosol parameters, combined with HONO DOAS fitting window optimisation, provide confidence in retrievals of aerosol extinction, NO_2 and HONO using the HEIPRO algorithm. The NO_2 results are comparable to the EPA air quality monitoring carried out around Melbourne, with average maximum NO_2 ~~levels for the three month measurement period around~~ at 8 ppb. Despite the moderate to low NO_2 pollution levels, high daytime HONO was commonly recorded with peak values in the late morning around 220 ppt. Such a consistent daytime HONO diurnal peak has previously been reported only in rural areas, and matches previously calculated diurnal profiles for a HONO missing source~~.~~, which was found here to have a production rate 1 $ppb.h^{-1}$ above the photostationary state HONO concentration. While strong vertical and temporal correlations between HONO and NO_2 exist generally, the correlation does not hold between weekends and weekdays ~~, suggesting that some of the high HONO levels are decoupled from~~ and ground based NO_2 conversion rates are insufficient to bridge the midday unknown HONO source gap. Strong relationships between solar radiation and HONO and strong HONO vertical gradients support previous theories that the missing HONO source is photolytically active and ground based. Furthermore, a dependence of both NO_2 and HONO on ~~the time since significant rainfall~~ soil moisture content suggests that soil ~~moisture~~ emissions may be playing an important role in the local ~~nitrogen oxide~~ reactive nitrogen chemistry. These findings suggest that HONO ~~may be~~ is significantly increasing the local tropospheric oxidation capacity, ~~providing~~ with an OH radical source ~~5-10 times greater in the middle of the day~~ strength up to four times stronger in the lowest 500 m of the troposphere than from ozone photolysis~~alone~~. Future studies ~~should further explore the relationship of different species in the oxidative cycle to the~~ in the Melbourne area should explore the oxidative cycles of HONO and OH ~~predicted from this work. Measurement of absolute OH radical concentrations and other nitrogen oxide species such as nitrates, would allow a more detailed analysis of the expected HONO pathways and mechanisms for the strong daytime HONO source observed~~involving soil processes. Through analysis of VOC oxidation processes and ozone, in

addition the reactive nitrogen cycle, future studies using MAX-DOAS should work towards a more complete understanding of vertical, spatial and temporal variations in tropospheric oxidation chemistry.

Author contributions. SR and MT maintained the MAX-DOAS instrument collecting the data. RR conducted the data analysis and drafted the manuscript. RR, SW, NJ, UF and RS contributed to developing the scientific direction, analysis protocols and writing the manuscript.

Competing interests. The authors declare that no competing interests exist.

Acknowledgements. RR wishes to acknowledge helpful discussions with Prof. Peter Rayner on atmospheric inverse methods and Dr Johannes Lampel on DOAS fitting methods, as well as Paul Torre and the Victorian Environment Protection Agency for making data air quality available. RS and RR acknowledge support from Australian Research Council's Centre of Excellence for Climate System Science (CE110001028) and Australian Research Council's Discovery project: Tackling Atmospheric Chemistry Grand Challenges in the Southern Hemisphere (DP160101598).

References

Acker, K. and Möller, D.: Atmospheric variation of nitrous acid at different sites in Europe, Environmental Chemistry, 4, 242–255 1449–8979, 2007.

Acker, K., Moller, D., Wieprecht, W., Meixner, F. X., Bohn, B., Gilge, S., PlassDülmer, ChristianDulmer, C., and Berresheim, H.: Strong daytime production of OH from HNO2 at a rural mountain site, Geophysical Research Letters, 33, 2006.

Atkinson, R., Baulch, D. L., Cox, R. A., Crowley, J. N., Hampson, R. F., Hynes, R. G., Jenkin, M. E., Rossi, M. J., and Troe, J.: Evaluated kinetic and photochemical data for atmospheric chemistry: Volume I - gas phase reactions of O_x, HO_x, NO_x and SO_x species, Atmospheric Chemistry and Physics, 4, 1461–1738, 2004.

Barnett, A. G., Williams, G. M., Schwartz, J., Best, T. L., Neller, A. H., Petroeschevsky, A. L., and Simpson, R. W.: The effects of air pollution on hospitalizations for cardiovascular disease in elderly people in Australian and New Zealand cities, Environmental health perspectives, 114, 1018, 2006.

Clémer, K., Van Roozendael, M., Fayt, C., Hendrick, F., Hermans, C., Pinardi, G., Spurr, R., Wang, P., and De Mazière, M.: Multiple wavelength retrieval of tropospheric aerosol optical properties from MAXDOAS measurements in Beijing, Atmos. Meas. Tech., 3, 863–878, https://doi.org/10.5194/amt-3-863-2010, https://www.atmos-meas-tech.net/3/863/2010/, 2010.

Creasey, D., Evans, G., Heard, D., and Lee, J.: Measurements of OH and HO2 concentrations in the Southern Ocean marine boundary layer, Journal of Geophysical Research: Atmospheres, 108, 2003.

DEE: Better fuel for cleaner air – draft regulation impact statement, Tech. rep., Department of the Environment and Energy, Australian Government, 2018.

Elshorbany, Y., Kurtenbach, R., Wiesen, P., Lissi, E., Rubio, M., Villena, G., Gramsch, E., Rickard, A., Pilling, M., and Kleffmann, J.: Oxidation capacity of the city air of Santiago, Chile, Atmospheric Chemistry and Physics, 9, 2257–2273

EPA, V.: Future air quality in Victoria Future air quality in Victoria – Final report, Tech. rep., Environmental Protection Agency Victoria, 2013.

Feister, U. and Grewe, R.: Spectral albedo measurements in the UV and visible region over different types of surfaces, Photochemistry and Photobiology, 62, 736–744

Finlayson-Pitts, B. J. and Pitts Jr, J. N.: Chemistry of the upper and lower atmosphere: theory, experiments, and applications, Academic Press, 1999.

Fleischmann, O. C., Hartmann, M., Burrows, J. P., and Orphal, J.: New ultraviolet absorption cross-sections of BrO at atmospheric temperatures measured by time-windowing Fourier transform spectroscopy, Journal of Photochemistry and Photobiology A: Chemistry, 168, 117–132 2004.

Frieß, U., Monks, P. S., Remedios, J. J., Rozanov, A., Sinreich, R., Wagner, T., and Platt, U.: MAX-DOAS O4 measurements: A new technique to derive information on atmospheric aerosols: 2. Modeling studies, Journal of Geophysical Research: Atmospheres, 111, 2006.

Garcia-Nieto, D., Benavent, N., and Saiz-Lopez, A.: Measurements of atmospheric HONO vertical distribution and temporal evolution in Madrid (Spain) using the MAX-DOAS technique, Science of The Total Environment, 643, 957–966, https://doi.org/https://doi.org/10.1016/j.scitotenv.2018.06.180, http://www.sciencedirect.com/science/article/pii/S0048969718322563, 2018.

George, C., Strekowski, R., Kleffmann, J., Stemmler, K., and Ammann, M.: Photoenhanced uptake of gaseous NO 2 on solid organic compounds: a photochemical source of HONO?, Faraday Discussions, 130, 195–210, 2005.

Grainger, J. F. and Ring, J.: Anomalous Fraunhofer Line Profiles, Nature, 193, 762–762, 1962.

Hafeez, F., Frost, A., Vaze, J., Dutta, D., Smith, A., and Elmahdi, A.: A new integrated continental hydrological simulation system, Water: Journal of the Australian Water Association, 42, 75, 2015.

Hendrick, F., Müller, J.-F., Clémer, K., Wang, P., Mazière, M. D., Fayt, C., Gielen, C., Hermans, C., Ma, J., and Pinardi, G.: Four years of ground-based MAX-DOAS observations of HONO and NO 2 in the Beijing area, Atmospheric Chemistry and Physics, 14, 765–781

Hermans, C., Vandaele, A., Fally, S., Carleer, M., Colin, R., Coquart, B., Jenouvrier, A., and Merienne, M.-F.: Absorption cross-section of the collision-induced bands of oxygen from the UV to the NIR, pp. 193–202, Springer, 2003.

Hönninger, G., von Friedeburg, C., and Platt, U.: Multi axis differential optical absorption spectroscopy (MAX-DOAS), Atmos. Chem. Phys., 4, 231–254, 2004.

Huang, R.-J., Yang, L., Cao, J., Wang, Q., Tie, X., Ho, K.-F., Shen, Z., Zhang, R., Li, G., and Zhu, C.: Concentration and sources of atmospheric nitrous acid (HONO) at an urban site in Western China, Science of The Total Environment, 593, 165–172, 2017.

Jin, J., Ma, J., Lin, W., Zhao, H., Shaiganfar, R., Beirle, S., and Wagner, T.: MAX-DOAS measurements and satellite validation of tropospheric NO2 and SO2 vertical column densities at a rural site of North China, Atmospheric Environment, 133, 12–25, 2016.

Kanaya, Y., Irie, H., Takashima, H., Iwabuchi, H., Akimoto, H., Sudo, K., Gu, M., Chong, J., Kim, Y., and Lee, H.: Long-term MAX-DOAS network observations of NO2 in Russia and Asia (MADRAS) during the period 2007–2012: instrumentation, elucidation of climatology, and comparisons with OMI satellite observations and global model simulations, Atmos. Chem. Phys, 14, 7909–7927, 2014.

Kleffmann, J.: Daytime sources of nitrous acid (HONO) in the atmospheric boundary layer, ChemPhysChem, 8, 1137–1144

Kleffmann, J., Kurtenbach, R., Lörzer, J., Wiesen, P., Kalthoff, N., Vogel, B., and Vogel, H.: Measured and simulated vertical profiles of nitrous acid—Part I: Field measurements, Atmospheric Environment, 37, 2949–2955 1352–2310, 2003.

Kleffmann, J., Lörzer, J., Wiesen, P., Kern, C., Trick, S., Volkamer, R., Rodenas, M., and Wirtz, K.: Intercomparison of the DOAS and LOPAP techniques for the detection of nitrous acid (HONO), Atmospheric Environment, 40, 3640–3652, 2006.

Lampel, J., Frieß, U., and Platt, U.: The impact of vibrational Raman scattering of air on DOAS measurements of atmospheric trace gases, Atmospheric Measurement Techniques, 8, 3767

Lampel, J., Pöhler, D., Polyansky, O. L., Kyuberis, A. A., Zobov, N. F., Tennyson, J., Lodi, L., Frieß, U., Wang, Y., and Beirle, S.: Detection of water vapour absorption around 363 nm in measured atmospheric absorption spectra and its effect on DOAS evaluations, Atmospheric Chemistry and Physics, 17, 1271–1295

Lee, J., Whalley, L., Heard, D., Stone, D., Dunmore, R., Hamilton, J., Young, D., Allan, J., Laufs, S., and Kleffmann, J.: Detailed budget analysis of HONO in central London reveals a missing daytime source, Atmospheric Chemistry and Physics, 16, 2747–2764, 2016.

Li, X., Brauers, T., Hofzumahaus, A., Lu, K., Li, Y., Shao, M., Wagner, T., and Wahner, A.: MAX-DOAS measurements of NO 2, HCHO and CHOCHO at a rural site in Southern China, Atmospheric Chemistry and Physics, 13, 2133–2151 1680–7316, 2013.

Li, X., Brauers, T., Häseler, R., Bohn, B., Fuchs, H., Hofzumahaus, A., Holland, F., Lou, S., Lu, K., and Rohrer, F.: Exploring the atmospheric chemistry of nitrous acid (HONO) at a rural site in Southern China, Atmospheric Chemistry and Physics, 12, 1497–1513, 2012.

Li, X., Rohrer, F., Hofzumahaus, A., Brauers, T., Häseler, R., Bohn, B., Broch, S., Fuchs, H., Gomm, S., and Holland, F.: Missing gas-phase source of HONO inferred from Zeppelin measurements in the troposphere, Science, 344, 292–296, 2014.

Ma, J., Beirle, S., Jin, J., Shaiganfar, R., Yan, P., and Wagner, T.: Tropospheric NO 2 vertical column densities over Beijing: results of the first three years of ground-based MAX-DOAS measurements (2008–2011) and satellite validation, Atmospheric Chemistry and Physics, 13, 1547–1567 1680–7316, 2013.

Madronich, S. and Flocke, S.: The role of solar radiation in atmospheric chemistry, pp. 1–26, Springer, 1999.

Meller, R. and Moortgat, G. K.: Temperature dependence of the absorption cross sections of formaldehyde between 223 and 323 K in the wavelength range 225–375 nm, Journal of Geophysical Research: Atmospheres, 105, 7089–7101 2156–2202, 2000.

Meusel, H., Kuhn, U., Reiffs, A., Mallik, C., Harder, H., Martinez, M., Schuladen, J., Bohn, B., Parchatka, U., and Crowley, J. N.: Daytime formation of nitrous acid at a coastal remote site in Cyprus indicating a common ground source of atmospheric HONO and NO, Atmospheric Chemistry and Physics, 16, 14 475–14 493

Meusel, H., Tamm, A., Kuhn, U., Wu, D., Leifke, A. L., Fiedler, S., Ruckteschler, N., Yordanova, P., Lang-Yona, N., and Pöhlker, M.: Emission of nitrous acid from soil and biological soil crusts represents an important source of HONO in the remote atmosphere in Cyprus, Atmospheric Chemistry and Physics, 18, 799–813

Michoud, V., Colomb, A., Borbon, A., Miet, K., Beekmann, M., Camredon, M., Aumont, B., Perrier, S., Zapf, P., and Siour, G.: Study of the unknown HONO daytime source at a European suburban site during the MEGAPOLI summer and winter field campaigns, Atmospheric Chemistry and Physics, 14, 2805–2822 1680–7316, 2014.

Neuman, J., Trainer, M., Brown, S., Min, K., Nowak, J., Parrish, D., Peischl, J., Pollack, I., Roberts, J., and Ryerson, T.: HONO emission and production determined from airborne measurements over the Southeast US, Journal of Geophysical Research: Atmospheres, 121, 9237–9250, 2016.

Ortega, I., Koenig, T., Sinreich, R., Thomson, D., and Volkamer, R.: The CU 2-D-MAX-DOAS instrument – Part 1: Retrieval of 3-D distributions of NO2 and azimuth-dependent OVOC ratios, Atmos. Meas. Tech., 8, 2371–2395, 2015.

Ortega, I., Berg, L. K., Ferrare, R. A., Hair, J. W., Hostetler, C. A., and Volkamer, R.: Elevated aerosol layers modify the O2–O2 absorption measured by ground-based MAX-DOAS, Journal of Quantitative Spectroscopy and Radiative Transfer, 176, 34–49, 2016.

Oswald, R., Behrendt, T., Ermel, M., Wu, D., Su, H., Cheng, Y., Breuninger, C., Moravek, A., Mougin, E., and Delon, C.: HONO emissions from soil bacteria as a major source of atmospheric reactive nitrogen, Science, 341, 1233–1235 0036–8075, 2013.

Pearce, J. L., Beringer, J., Nicholls, N., Hyndman, R. J., Uotila, P., and Tapper, N. J.: Investigating the influence of synoptic-scale meteorology on air quality using self-organizing maps and generalized additive modelling, Atmospheric Environment, 45, 128–136, 2011.

Pinto, J., Dibb, J., Lee, B., Rappengluck, B., Wood, E., Levy, M., Zhang, R.-Y., Lefer, B., Ren, X.-R., and Stutz, J.: Intercomparison of field measurements of nitrous acid (HONO) during the SHARP campaign, Journal of Geophysical Research: Atmospheres, 119, 5583–5601, 2014.

Platt, U. and Perner, D.: Measurements of atmospheric trace gases by long path differential UV/visible absorption spectroscopy, pp. 97–105, Springer, 1983.

Platt, U. and Stutz, J.: Differential Optical Absorption Spectroscopy, Springer-Verlag Berlin Heidelberg, Berlin, 2008.

Pusede, S. E., VandenBoer, T. C., Murphy, J. G., Markovic, M. Z., Young, C. J., Veres, P. R., Roberts, J. M., Washenfelder, R. A., Brown, S. S., and Ren, X.: An atmospheric constraint on the NO2 dependence of daytime near-surface nitrous acid (HONO), Environmental Science & Technology, 49, 12 774–12 781, 2015.

Qin, M., Xie, P., Su, H., Gu, J., Peng, F., Li, S., Zeng, L., Liu, J., Liu, W., and Zhang, Y.: An observational study of the HONO–NO2 coupling at an urban site in Guangzhou City, South China, Atmospheric Environment, 43, 5731–5742, 2009.

Qin, Y. and Mitchell, R.: Characterisation of episodic aerosol types over the Australian continent, Atmospheric Chemistry and Physics, 9, 1943–1956 1680–7316, 2009.

Ren, X., Harder, H., Martinez, M., Lesher, R. L., Oliger, A., Simpas, J. B., Brune, W. H., Schwab, J. J., Demerjian, K. L., and He, Y.: OH and HO2 chemistry in the urban atmosphere of New York City, Atmospheric Environment, 37, 3639–3651

Rodgers, C. D.: Characterization and error analysis of profiles retrieved from remote sounding measurements, Journal of Geophysical Research: Atmospheres, 95, 5587–5595, 1990.

Rodgers, C. D.: Inverse methods for atmospheric sounding: theory and practice, vol. 2, World scientific, 2000.

Roscoe, H. K., Van Roozendael, M., Fayt, C., du Piesanie, A., Abuhassan, N., Adams, C., Akrami, M., Cede, A., Chong, J., Clémer, K., Friess, U., Gil Ojeda, M., Goutail, F., Graves, R., Griesfeller, A., Grossmann, K., Hemerijckx, G., Hendrick, F., Herman, J., Hermans, C., Irie, H., Johnston, P. V., Kanaya, Y., Kreher, K., Leigh, R., Merlaud, A., Mount, G. H., Navarro, M., Oetjen, H., Pazmino, A., Perez-Camacho, M., Peters, E., Pinardi, G., Puentedura, O., Richter, A., Schönhardt, A., Shaiganfar, R., Spinei, E., Strong, K., Takashima, H., Vlemmix, T., Vrekoussis, M., Wagner, T., Wittrock, F., Yela, M., Yilmaz, S., Boersma, F., Hains, J., Kroon, M., Piters, A., and Kim, Y. J.: Intercomparison of slant column measurements of NO_2 and O_4 by MAX-DOAS and zenith-sky UV and visible spectrometers, Atmospheric Measurement Techniques, 3, 1629–1646, 2010.

Rozanov, V., Rozanov, A., Kokhanovsky, A., and Burrows, J.: Radiative transfer through terrestrial atmosphere and ocean: Software package {SCIATRAN}, Journal of Quantitative Spectroscopy and Radiative Transfer, 133, 13 – 71, https://doi.org/http://dx.doi.org/10.1016/j.jqsrt.2013.07.004, http://www.sciencedirect.com/science/article/pii/S0022407313002872, 2014.

Sander, S., Golden, D., Kurylo, M., Moortgat, G., Wine, P., Ravishankara, A., Kolb, C., Molina, M., Finlayson-Pitts, B., and Huie, R.: Chemical kinetics and photochemical data for use in atmospheric studies evaluation number 15, Tech. rep., 2006.

Schreier, S. F., Richter, A., Wittrock, F., and Burrows, J. P.: Estimates of free-tropospheric NO2 and HCHO mixing ratios derived from high-altitude mountain MAX-DOAS observations at midlatitudes and in the tropics, Atmospheric Chemistry & Physics, 16, 2803–2817, 2016.

Serdyuchenko, A., Gorshelev, V., Weber, M., Chehade, W., and Burrows, J.: High spectral resolution ozone absorption cross-sections, Atmospheric Measurement Techniques, 7, 1867–8548, 2014.

Simpson, R., Denison, L., Petroeschevsky, A., Thalib, L., and Williams, G.: Effects of ambient particle pollution on daily mortality in Melbourne, 1991-1996, Journal of Exposure Science and Environmental Epidemiology, 10, 1559–0631, 2000.

Simpson, R., Williams, G., Petroeschevsky, A., Best, T., Morgan, G., Denison, L., Hinwood, A., Neville, G., and Neller, A.: The short term effects of air pollution on daily mortality in four Australian cities, Australian and New Zealand journal of public health, 29, 205–212, 2005.

Stemmler, K., Ammann, M., Donders, C., Kleffmann, J., and George, C.: Photosensitized reduction of nitrogen dioxide on humic acid as a source of nitrous acid, Nature, 440, 195

Stutz, J., Kim, E., Platt, U., Bruno, P., Perrino, C., and Febo, A.: UV visible absorption cross sections of nitrous acid, Journal of Geophysical Research: Atmospheres, 105, 14 585–14 592, 2000.

Stutz, J., Oh, H.-J., Whitlow, S. I., Anderson, C., Dibb, J. E., Flynn, J. H., Rappengluck, B., and Lefer, B.: Simultaneous DOAS and mist-chamber IC measurements of HONO in Houston, TX, Atmospheric Environment, 44, 4090–4098, 2010.

Su, H., Cheng, Y., Oswald, R., Behrendt, T., Trebs, I., Meixner, F. X., Andreae, M. O., Cheng, P., Zhang, Y., and Pöschl, U.: Soil nitrite as a source of atmospheric HONO and OH radicals, Science, 333, 1616–1618 0036–8075, 2011.

Thalman, R. and Volkamer, R.: Temperature dependent absorption cross-sections of O 2–O 2 collision pairs between 340 and 630 nm and at atmospherically relevant pressure, Physical chemistry chemical physics, 15, 15 371–15 381, 2013.

Vandaele, A. C., Hermans, C., Simon, P. C., Carleer, M., Colin, R., Fally, S., Merienne, M.-F., Jenouvrier, A., and Coquart, B.: Measurements of the NO2 absorption cross-section from 42 000 cm-1 to 10 000 cm-1 (238–1000 nm) at 220 K and 294 K, Journal of Quantitative Spectroscopy and Radiative Transfer, 59, 171–184, 1998.

VandenBoer, T., Markovic, M., Sanders, J., Ren, X., Pusede, S., Browne, E., Cohen, R., Zhang, L., Thomas, J., and Brune, W.: Evidence for a nitrous acid (HONO) reservoir at the ground surface in Bakersfield, CA, during CalNex 2010, Journal of Geophysical Research: Atmospheres, 119, 9093–9106 2169–8996, 2014.

VandenBoer, T. C., Brown, S. S., Murphy, J. G., Keene, W. C., Young, C. J., Pszenny, A., Kim, S., Warneke, C., Gouw, J. A., and Maben, J. R.: Understanding the role of the ground surface in HONO vertical structure: High resolution vertical profiles during NACHTT11, Journal of Geophysical Research: Atmospheres, 118, 2013.

VandenBoer, T. C., Young, C. J., Talukdar, R. K., Markovic, M. Z., Brown, S. S., Roberts, J. M., and Murphy, J. G.: Nocturnal loss and daytime source of nitrous acid through reactive uptake and displacement, Nature Geoscience, 8, 55

Vlemmix, T., Hendrick, F., Pinardi, G., De Smedt, I., Fayt, C., Hermans, C., Piters, A., Wang, P., Levelt, P., and Van Roozendael, M.: MAX-DOAS observations of aerosols, formaldehyde and nitrogen dioxide in the Beijing area: comparison of two profile retrieval approaches, Atmos. Meas. Tech., 8, 941–963, 2015.

Vogel, L., Sihler, H., Lampel, J., Wagner, T., and Platt, U.: Retrieval interval mapping: a tool to visualize the impact of the spectral retrieval range on differential optical absorption spectroscopy evaluations, Atmospheric Measurement Techniques, 6, 275–299

Volkamer, R., Baidar, S., Campos, T. L., Coburn, S., DiGangi, J. P., Dix, B., Eloranta, E. W., Koenig, T. K., Morley, B., and Ortega, I.: Aircraft measurements of BrO, IO, glyoxal, NO 2, H 2 O, O 2–O 2 and aerosol extinction profiles in the tropics: Comparison with aircraft-/ship-based in situ and lidar measurements, Atmospheric Measurement Techniques, 8, 2121 1867–8548, 2015.

Wagner, T., Dix, B., Friedeburg, C. v., Frieß, U., Sanghavi, S., Sinreich, R., and Platt, U.: MAX-DOAS O4 measurements: A new technique to derive information on atmospheric aerosols—Principles and information content, Journal of Geophysical Research: Atmospheres, 109, 2004.

Wagner, T., Beirle, S., Brauers, T., Deutschmann, T., Frieß, U., Hak, C., Halla, J., Heue, K., Junkermann, W., and Li, X.: Inversion of tropospheric profiles of aerosol extinction and HCHO and NO 2 mixing ratios from MAX-DOAS observations in Milano during the summer of 2003 and comparison with independent data sets, Atmospheric Measurement Techniques, 4, 2685–2715 1867–1381, 2011.

Wagner, T., Beirle, S., Remmers, J., Shaiganfar, R., and Wang, Y.: Absolute calibration of the colour index and O4 absorption derived from Multi-AXis (MAX-) DOAS measurements and their application to a standardised cloud classification algorithm, Atmos. Meas. Tech. Discuss., 2016, 1–34, 2016.

Wang, S., Cuevas, C. A., Frieß, U., and Saiz-Lopez, A.: MAX-DOAS retrieval of aerosol extinction properties in Madrid, Spain, Atmos. Meas. Tech. Discuss., 2016, 1–26, 2016.

Wang, Y., Beirle, S., Hendrick, F., Hilboll, A., Jin, J., Kyuberis, A. A., Lampel, J., Ang, L., Luo, Y., and Lodi, L.: MAX-DOAS measurements of HONO slant column densities during the MAD-CAT campaign: inter-comparison, sensitivity studies on spectral analysis settings, and error budget, Atmospheric Measurement Techniques, 10, 1867–8548, 2017.

Weber, B., Wu, D., Tamm, A., Ruckteschler, N., Rodríguez-Caballero, E., Steinkamp, J., Meusel, H., Elbert, W., Behrendt, T., and Soergel, M.: Biological soil crusts accelerate the nitrogen cycle through large NO and HONO emissions in drylands, Proceedings of the National Academy of Sciences, 112, 15 384–15 389

WHO: Ambient air pollution: A global assessment of exposure and burden of disease, Tech. rep., World Health Organisation, 2016.

Wilson, S.: Characterisation of J (O1D) at Cape Grim 2000-2005, Atmospheric Chemistry and Physics Discussions, 14, 18 389–18 419, 2015.

Wojtal, P., Halla, J., and McLaren, R.: Pseudo steady states of HONO measured in the nocturnal marine boundary layer: a conceptual model for HONO formation on aqueous surfaces, Atmospheric Chemistry and Physics, 11, 3243–3261 1680–7316, 2011.

Wong, K., Tsai, C., Lefer, B., Haman, C., Grossberg, N., Brune, W., Ren, X., Luke, W., and Stutz, J.: Daytime HONO vertical gradients during SHARP 2009 in Houston, TX, Atmospheric Chemistry and Physics, 12, 635–652, 2012.

Ye, C., Heard, D. E., and Whalley, L. K.: Evaluation of Novel Routes for NOx Formation in Remote Regions, Environmental Science & Technology, 51, 7442–7449, 2017.

Young, C. J., Washenfelder, R. A., Roberts, J. M., Mielke, L. H., Osthoff, H. D., Tsai, C., Pikelnaya, O., Stutz, J., Veres, P. R., and Cochran, A. K.: Vertically resolved measurements of nighttime radical reservoirs in Los Angeles and their contribution to the urban radical budget, Environmental Science & Technology, 46, 10 965–10 973

Zhou, X., Zhang, N., TerAvest, M., Tang, D., Hou, J., Bertman, S., Alaghmand, M., Shepson, P. B., Carroll, M. A., and Griffith, S.: Nitric acid photolysis on forest canopy surface as a source for tropospheric nitrous acid, Nature Geoscience, 4, 1752–0908, 2011.